Optimising Fuel Consumption in Thrust Allocation for Marine Dynamic Positioning Systems

Miltiadis Kalikatzarakis, *Member, IEEE,* Andrea Coraddu, *Member, IEEE,*
Luca Oneto, *Member, IEEE,* Davide Anguita, *Senior Member, IEEE*

***Abstract*—In offshore maritime operations, automated systems capable to maintain the vessel's position and heading using its own propellers and thrusters to compensate exogenous disturbances, like wind, waves and currents, are referred to as Marine Dynamic Positioning (DP) Systems. DP systems play a central role in assuring the mission of the vessels, such as for drilling, pipe-laying, coring, and ocean observation operations. At the same time, vessels operations are the primary cause of fuel consumption, having a strong impact on the overall footprint of the vessel. For this reason, in this paper, we will face the problem of optimising the propellers thrust allocation, namely determining thrust and direction of each propeller and thruster in an over-actuated vessel, to maintain its position and heading, while minimising the fuel consumption. State of the art approaches simplify this problem by roughly approximating it and obtain a simple, mostly convex, optimisation problem. This allows to solve it in near-real time allowing its exploitation on-board during operation by simply integrating it in the automation system. In this paper, we deal with the problem of improving the current approaches with a twofold contribution. On one hand, we will exploit a detailed modelling approach of the physical system, resulting in an high fidelity representation of the optimisation problem. On the other hand, we will study and manipulate the resulting optimisation problem in such a way that it is still possible to solve it in near-real time on conventional on-board computing platform. Authors will leverage on a Platform Supply Vessel, equipped with 6 thrusters, as case study to evaluate the quality of the proposal. Results will show that, leveraging on the proposed approach, it is possible to achieve up to 5% of fuel savings with respect to conventional approaches.**

***Note to Practitioners*—This paper was motivated by the problem of minimising the fuel consumption in thrust allocation for marine dynamic positioning systems. Current approaches commonly exploit a simplified approach where simpler, yet related, optimisation problems are exploited as surrogates to keep the problem and the computational requirements at a level suited for a near-real time control. We propose, instead, to face the original problem with a state-of-the-art modelisation of the physical system and exploit reasonable and theoretical proprietaries for the purpose of achieving optimal solutions in near-real time. Results on a Platform Supply Vessel will show savings in fuel consumption of up to 5% with respect to using state-of-the-art alternative approaches.**

***Index Term*— Marine Dynamic Positioning Systems, Thrust Allocation Problem, Fuel Consumption Optimisation, Near Real Time Optimisation**

I. Introduction

A vessel equipped with a Dynamic Positioning (DP) system is able to maintain a fixed position and heading by using exclusively its thrusters and propellers [1]. This capability is critical in several maritime operations such as offshore drilling, coring, undersea pipe-laying operations, and dredging [2]. Moreover, in offshore support vessels that need to maintain close, but safe, distance from offshore platforms [3]. The same applies to offloading process of Floating Production Storage and Offloading units (FPSOs) [4]. These operations experienced an increase in demand and complexity during the last decades [5]. Consequently, there is the necessity to design and operate more an more sophisticated DP systems, capable of providing the required manoeuvring precision, operational, environmental efficiency, and durability [6]. Over the past 70 years, these requirements have motivated the research community to study and develop increasingly sophisticated DP controllers. Starting from the simple Proportional-Integral-Derivative (PID) controllers aiming to compensate horizontal modes of motion (surge, sway and yaw), DP systems evolved into highly sophisticated tools leveraging on multivariate optimal controls and Kalman filtering [7]–[14], non-linear or model predictive controls [2], [15]–[20], hybrid [21]–[24] or fault-tolerant controls [25]–[27]. A detailed review of the early history of DP systems is reported in [28], whereas the latest comprehensive surveys on technology advancements can be found in [29]–[31].

In the context of DP systems one has to handle two different scenarios. In the ideal case, namely the design or the retrofitting of a vessel, it is possible to contemporary optimise the design of the propulsion and the control systems for DP purposes. In particular, among other tasks, the control system needs to solve the so called thrust allocation problem [1], in order to ensure the vessels' position and heading using its own propellers and thrusters to compensate exogenous disturbances. This first scenario has obviously a remarkable impact in terms of costs and operational time (in case of retrofitting). In a more realistic scenario it necessary to improve the operations acting just on the control systems. This second scenario is surely sub-optimal and more complex but is cost effective and has a negligible impact on the operational time. It is worth noting that the tools developed in the second scenario apply also to the first scenario. Indeed, an effective thrust allocation algorithm can guide the design of propulsion systems which allows to minimise the fuel consumption, and/or the cost and/or the complexity of a DP-focused propulsive layout [32].

Therefore, in this work, authors focused on the second scenario. Currently, the design of an effective thrust allocation algorithms needs to address a multi-objective optimisation problem [30]. On the one hand we have to ensure the vessel position and heading in the most possible severe conditions

Miltiadis Kalikatzarakis and Andrea Coraddu are with the Department of Naval Architecture, Ocean & Marine Engineering, University of Strathclyde, Glasgow, G1 1SJ UK {miltiadis.kalikatzarakis,andrea.coraddu}@strath.ac.uk Luca Oneto and Davide Anguita are with the DIBRIS Department, University of Genova, Via Opera Pia 11a, 16145 Genova, Italy (email: {Luca.Oneto, Davide.Anguita}@unige.it)

taking into account the physical limitations of all related components, on the other hand we need to minimise the environmental footprint by minimising the fuel consumption. Contemporary, the DP control system needs to run smoothly on the on-board automation platform in near-real time, being able to promptly react to the evolution of the dynamical system. In literature, it is possible to find a large variety of multi-objective cost functions and constraints for thrust allocation

- minimisation of electrical load fluctuations [33];
- minimisation of total required power [6], [34]–[37];
- maximisation of thrust production efficiency [38];
- minimisation of fuel consumption [39]–[41];
- constraints on thrust production due to physical equipment's limits [1], [6], [34], [42], [43];
- constraints of rudder dynamics which limit the number of combinations of propeller thrust directions [1], [44];
- constraints for the safe operations of thrusters and steering machines [1], [6], [34], [45];
- constraints on forbidden thrust production zones to reduce thrust losses [1], [34], [38], [45],
- constraints on thrust allocation schemes for moments in the roll and pitch motions which are fundamental for vessels with large draft and beam with respect to overall length [1].

Based on this literature review, the environmental footprint, and then the fuel consumption, minimisation is one of the most challenging and unexplored area of research. Authors in [46] discuss this problem for the Varg FPSO unit and the West Venture drilling rig. However the authors just focused on Power Management Strategy (PMS) which is responsible for the allocation of power among the Diesel Generator sets (DGs). In particular, the authors considered power production and power demand as two separate problems, without coupling them. Analogously, the authors of [47] developed a PMS able to minimise operational costs and improve fuel consumption of the DP system, purely from the PMS point of view. This gap in the literature has been also pointed out in [39], [40]. In particular, authors of [39] exploited a Platform Supply Vessel to investigate the possibility of using the thrust allocation algorithm to minimise, in near-real time, the fuel consumption of the DG sets. The authors formulated the thrust optimisation problem as a standard convex Quadratic Programming (QP) one, by simplifying the original formulation roughly approximating the involved objectives and constraints with linear and quadratic functions around the vessel's operating point. The authors demonstrated that their proposal can lead to up to 2% in fuel savings with respect to the thrust allocation which minimises simply the thrust power. Authors of [40] exploited a turret-moored assisted FPSO as a case study, and a thrust allocation algorithm was developed to minimise fuel consumption based on penalty programming. Also in this case, the fuel consumption of the online DG sets was approximated as a second degree polynomial with respect to power output. By using penalty programming, the authors reformulated the constrained optimisation problem by means a combination of unconstrained ones. The authors compared the proposed approach with other existing thrust allocation algorithms, and showed additional fuel savings up to 7%.

In this work, we will focus on fuel consumption minimisation during DP operations considering power supply and demand as a whole. The complexity of this task, and the novelty of this work, lies in finding the right trade-off between computational complexity and accuracy in representing the fuel consumption. As the authors will show in the following sections, this balance is accomplished by a series of theoretically founded simplifications, both in terms of the representation of the physical system itself, and during the formulation of the optimisation problem. Furthermore, we will quantify the effects of exploiting Controllable Pitch Propellers (CPPs), as an extra degree of freedom (DOF), in the optimisation problem. Finally, to demonstrate the quality of the proposed approach, we will compare against state-of-the-art methods [3], [33], [34], [37], [39], [43], [44], [48]–[55] where the minimisation of total thrust and total propeller power, with and without propeller pitch control, are proposed instead of directly optimising the fuel consumption.

Figure 1: Magellan Class drilling unit [56].

The rest of the paper is organised as follows. In Section II we present the case study exploited in this work, along with the modelling approach employed for the environmental conditions, the Diesel-electric propulsion, and the DP systems. Section III discusses the formulation of the thrust allocation problem and the associated proposed solution method. Sections IV present the results of applying the methodology proposed in Section III using the case study presented in Section II. Section V concludes the paper. Note that, to improve the readability of the paper, authors reported in Tables II and I, respectively, the summary of the acronyms and nomenclature exploited during the presentation.

II. The Case Study

In this section we will describe in detail the case study under consideration, and also provide the mathematical framework required to formulate the thrust allocation optimisation problem.

A. System Description

We considered the 89,800 ton Magellan Class drilling unit depicted in Figure 1. The main characteristics of the vessel are reported in Table III, while its Diesel-electric propulsion scheme is shown in Figure 2. The vessel is equipped with $k_p = 6$ azimuth thrusters. The layout is reported in Figure 3.

Any vessel in seaway is mainly affected by the different environmental disturbances, namely waves, currents, and wind,

Table I: List of symbols exploited in the paper.

Symbol	Description	Units	Symbol	Description	Units	Symbol	Description	Units
A_{Fw}	Frontal area projection	m^2	L_{pp}	Length between perpendiculars	m	$\boldsymbol{v_c}$	Current velocity vector	m/s
A_{Lw}	Lateral area projection	m^2	l_M	Mutual inductance	H	v_{ds}	Stator direct voltage	V
A_{wl}	Waterline area	m^2	l'_r	Rotor inductance	H	$v_{ds,ref}$	Stator direct voltage reference	V
$\boldsymbol{a_{max}}$	Maximum azimuth angle	rad	l'_{rr}	Rotor equivalent inductance	H	$v_{ds,set}$	Direct voltage setpoint	V
$\boldsymbol{a_{min}}$	Minimum azimuth angle	rad	l_s	Stator inductance	H	v'_{dr}	Rotor direct voltage	V
B	Breadth	m	l_{ss}	Stator equivalent inductance	H	v_{qs}	Stator quadrature voltage	V
C_{cn}	Current drag coefficient - yaw	-	$\boldsymbol{M}$	Vessel inertial matrix	kg	$v_{qs,ref}$	Stator quadrature voltage reference	V
C_{cx}	Current drag coefficient - surge	-	$\boldsymbol{M_{em}}$	Electric motor torque vector	Nm	$v_{qs,set}$	Quadrature voltage setpoint	V
C_{cy}	Current drag coefficient - sway	-	$M_{em,max}$	Maximum electric motor torque	Nm	v'_{qr}	Rotor quadrature voltage	V
C_q	Propeller torque coefficient	-	$\boldsymbol{M_{gb}}$	Gearbox torque vector	Nm	$\boldsymbol{v_{ref}}$	Voltage reference vector	V
C_t	Propeller thrust coefficient	-	$\boldsymbol{M_{gb,loss}}$	Gearbox torque loss vector	Nm	v_{rw}	Lateral relative wind velocity	m/s
$C_{wav,n}$	Current drag coefficient - yaw	-	$\boldsymbol{M_p}$	Propeller torque vector	Nm	$\boldsymbol{v_{set}}$	Voltage setpoint vector	V
$C_{wav,x}$	Current drag coefficient - surge	-	$\boldsymbol{M_{sh}}$	Shaft torque vector	Nm	w	Vessel lateral velocity	m/s
$C_{wav,y}$	Current drag coefficient - sway	-	$\boldsymbol{M_{sh,loss}}$	Shaft torque loss vector	Nm	$\boldsymbol{w}$	Exogenous inputs vector	-
C_{wn}	Wind drag coefficient - yaw	-	$\dot{m}_f$	Total fuel consumption	kg/s	w_c	Lateral current velocity	m/s
C_{wx}	Wind drag coefficient - surge	-	N_{dg}	No. of diesel generators connected	-	w_{rc}	Lateral relative current velocity	m/s
C_{wy}	Wind drag coefficient - sway	-	$N_{\dot{y}}$	Added mass force - yaw	N	$X_{\dot{u},\dot{v}}$	Added mass force - surge	N
$c_{ct,i}$	Thrust coefficient approx. constants	m/s	$\boldsymbol{n_p}$	Propeller rotational speed vector	Hz	x	Vessel longitudinal position	m
$c_{cq,i}$	Torque coefficient approx. constants	m/s	$\boldsymbol{n_{em}}$	Electric motor rotational speed	Hz	x_G	Distance of CoG and body-frame	m
$c_{dg,i}$	Fuel consumption approx. constants	-	$P_{dg,max}$	Maximum diesel generator power	W	$Y_{\dot{u},\dot{v}}$	Added mass force - sway	N
$\boldsymbol{D}$	Hydrodynamic force coefficients	kg/s	$\boldsymbol{P_p}$	Propeller power vector	W	y	Vessel lateral position	m
D	Depth	m	P_{tot}	Total propeller power	W	z	Vessel angular velocity	m/s
D_p	Propeller diameter	m	p_{max}	Maximum admissible pitch	m	$\boldsymbol{z_{dg}}$	Diesel-generator grid connection	-
$\boldsymbol{d_{dg}}$	Diesel generator pair connection	-	p_{min}	Minimum admissible pitch	m	$\boldsymbol{\alpha}$	Thruster angle vector	rad
F_n	Thruster moment	N	q	Electric motor pole pairs	-	$\boldsymbol{\beta}$	Hydrodynamic pitch angle	rad
F_x	Thruster longitudinal force	N	r'_r	Rotor resistance	Ω	γ_c	Current angle	rad
F_y	Thruster lateral force	N	r_s	Stator resistance	Ω	γ_{rc}	Relative current angle	rad
f	Objective function	-	$\boldsymbol{s_{fc}}$	Specific fuel consumption vector	g/kWh	γ_{rw}	Relative wind angle	rad
$\boldsymbol{f}$	Thruster force vector	N	T	Draft	m	γ_w	Wind angle	rad
$\boldsymbol{f_c}$	Current force vector	N	$T_{p,max}$	Maximum attainable thrust force	N	γ_{wav}	Wave angle	rad
$\boldsymbol{f_{env}}$	Environmental force vector	N	T_{tot}	Total propeller thrust	N	Δ	Displacement	kg
$\boldsymbol{f_w}$	Wind force vector	N	$\boldsymbol{T_{t,e}}$	Extended thrust configuration vector	-	$\boldsymbol{\eta_{em}}$	Electric motor efficiency vector	-
f_w	wake factor	-	u	Vessel longitudinal velocity	m/s	η_r	Relative rotative efficiency	-
$\boldsymbol{g}$	Inequality constraints vector	-	$\boldsymbol{u}$	Total control vector	-	ρ_a	Air density	kg/m^3
H_s	Significant wave height	m	u_c	Longitudinal current velocity	m/s	ρ_w	Water density	kg/m^3
$\boldsymbol{h}$	Equality constraints vector	-	$\boldsymbol{u_{dg}}$	Diesel-generator power output vector	W	σ_i	Grouped optimisation constants	-
$\boldsymbol{I_u}$	Current coefficient vector	-	$\boldsymbol{u_p}$	Propeller pitch vector	m	$\boldsymbol{\tau}$	Vessel position vector	m
I_z	Moment of inertial	$kg\ m^2$	u_{rc}	Longitudinal relative current velocity	m/s	ψ	Vessel heading	rad
i'_{dr}	Rotor direct current	A	u_{rw}	Longitudinal relative wind velocity	m/s	ψ'_{dr}	Rotor direct flux linkage	$Wb\ t$
i_{ds}	Stator direct current	A	$\boldsymbol{u_{t,e}}$	Thrust extended control vector	N	ψ_{ds}	Stator direct flux linkage	$Wb\ t$
$i_{ds,set}$	Stator direct current setpoint	A	$\boldsymbol{u_x}$	Thrust control vector - surge	N	ψ'_{qr}	Rotor quadrature flux linkage	$Wb\ t$
i'_{qr}	Rotor quadrature current	A	$\boldsymbol{u_y}$	Thrust control vector - sway	N	ψ_{qs}	Stator quadrature flux linkage	$Wb\ t$
i_{qs}	Stator quadrature current	A	V_{des}	Vessel design velocity	m/s	ω_b	Electric motor base frequency	rad/s
$i_{qs,set}$	Stator quadrature current setpoint	A	V_{rc}	Norm of relative current velocity	m/s	ω_e	Rotating reference frame frequency	rad/s
$\boldsymbol{J}$	Reference frame transformation matrix	-	V_{rw}	Norm of relative wind velocity	m/s	$\boldsymbol{\omega_{em}}$	Electric motor frequency	rad/s
$\boldsymbol{K_{t,e}}$	Diagonal force coefficient matrix	-	V_w	Sustained wind speed $10m$ above sea	m/s	ω_{mf}	Magnetic field frequency	rad/s
$\boldsymbol{K_u}$	Inductance coefficient vector	-	$\boldsymbol{v}$	Vessel velocity vector	m/s	ω_r	Electric rotor frequency	rad/s
L_{oa}	Length overall	m	v_a	Propeller advance velocity	m/s	ω_{sl}	Slip frequency	rad/s

Table II: List of acronyms exploited in the paper.

Acronym	Description
ALGA	Augmented Lagrangian Genetic Algorithm
BINLP	Binary Integer Non-linear Programming
C0G	Center of Gravity
CP	Capability Plot
CPP	Controllable Pitch Propeller
DG	Diesel Generator
DOF	Degrees of Freedom
DP	Dynamic Positioning
EM	Electric Motor
GA	Genetic Algorithm
GB	Gearbox
IPM	Interior Point Method
LSE	Least Square Errors
MAPE	Mean Absolute Percentage Error
MINLP	Mixed Integer Non-Linear Programming
PID	Proportional - Integral - Derivative
PMS	Power Management Strategy
PROP	Propeller
PSO	Particle Swarm Optimisation
QP	Quadratic Programming
SB	Switchboard
SVD	Singular Value Decomposition
TH	Thruster

Table III: Main characteristics of the Magellan Class drilling unit depicted in Figure 1.

Properties	Symbols	Values	Units
Length overall	L_{oa}	243	m
Length between perpendiculars	L_{pp}	232	m
Breadth at midship	B	39.8	m
Draft at midship	T	13	m
Depth moulded	D	19	m
Displacement	Δ	104,000	$tons$
Speed	V_{des}	13-16	kn
Waterline area	A_{wl}	7,500	m^2
Frontal area projection	A_{Fw}	2,093	m^2
Lateral area projection	A_{Lw}	7,500	m^2

which contain both slowly varying and high-frequency components [57]. For DP applications, by definition, the vessel is operating at close to zero speed, and only forces and moments in the horizontal plane are of interest [58]. We model the overall forces an moments using the principle of superposition, which is the most commonly adopted model for thrust allocation optimisation problem in DP [59].

- first order waves-induced motion;
- slowly varying disturbance motion produced by second order wave effects, current, and wind;
- control-induced motion produced by the thrusters.

However, the commercial autopilot and DP systems employed in real-world applications have various forms of wave filtering, such as cascaded notch and low-pass filters, to reduce wear and tear on both the steering machines and thrusters' modulation [1], [60]. Note that, only the slowly varying disturbances are counteracted by the steering and propulsion systems since

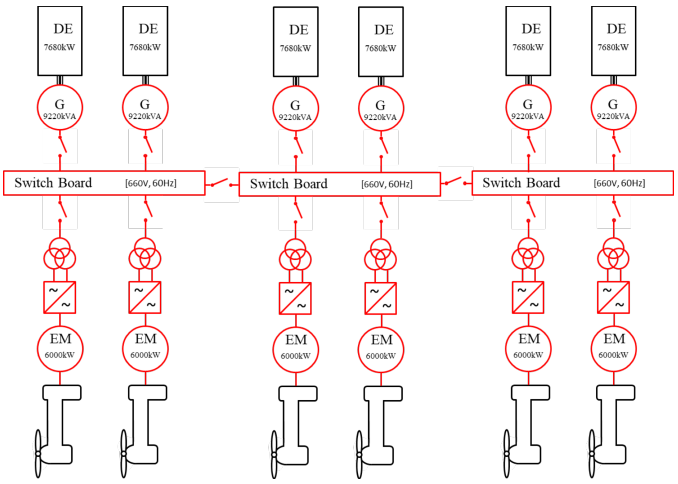

Figure 2: Diesel-electric propulsion scheme of the Magellan Class drilling unit depicted in Figure 1

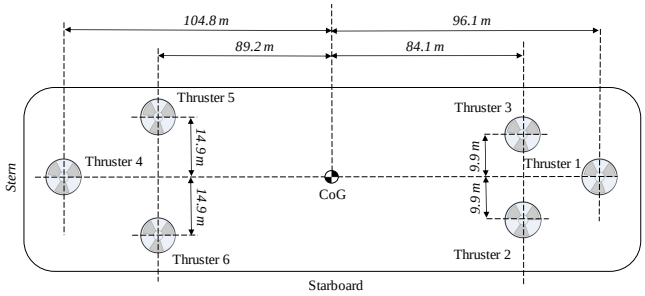

Figure 3: Thruster layout of the Magellan Class drilling unit depicted in Figure 1.

the oscillatory motion due to waves should not be considered in the control feedback loop, to avoid unnecessary usage of the actuators [1], [57]. Hence, in order to be able to model the system in the most realistic possible way, we assume that these filtering techniques have been successfully implemented in the control system by neglecting the oscillatory motion.

B. Vessel Kinematics

For low speed applications, it is common to consider the low frequency mathematical model in surge, sway, and yaw. The latter is dynamically linear and kinematically non-linear [1]. In this mathematical model, the pitch and roll angles are assumed to be small, the ship has port-starboard symmetry, the Coriolis and centripetal terms are negligible, and the linear part of the damping matrix caused by wave drift damping and laminar skin friction has a dominating contribution [58].

$$\dot{\boldsymbol{\tau}} = \boldsymbol{J}(\boldsymbol{\tau})\boldsymbol{v}, \tag{1}$$

$$\boldsymbol{M}\dot{\boldsymbol{v}} + \boldsymbol{D}\left(\boldsymbol{v} - \boldsymbol{v_c}\right) = \boldsymbol{f} + \boldsymbol{f_{env}}. \tag{2}$$

$\boldsymbol{\tau} = [x, y, \psi]^\intercal \in \mathbb{R}^{3\times 1}$ is the output vector containing the vessel's position (x, y) and heading (ψ) in the earth-fixed frame. $\boldsymbol{v} = [u, w, z]^\intercal \in \mathbb{R}^{3\times 1}$ contains the vessel's forward (u), lateral (w), and angular (z) velocities in the body-fixed frame. $\boldsymbol{v_c} = [u_c, w_c, 0]^\intercal \in \mathbb{R}^{3\times 1}$ is the current velocities vector, discussed in Section II-C. $\boldsymbol{f} = [f_x, f_y, f_n]^\intercal \in \mathbb{R}^{3\times 1}$ represents the forces and moment from the thrusters in the body-fixed frame (we will describe this later in Section II-D, specifically Eq. (12)). $\boldsymbol{f_{env}} \in \mathbb{R}^{3\times 1}$ represents the environmental disturbances coming from the wind, current, and waves (we will describe this later in Section II-C). $\boldsymbol{J} \in \mathbb{R}^{3\times 3}$ represents the transformation matrix from the vessel-fixed to the earth-fixed frame, according to Eq. (3). $\boldsymbol{M} \in \mathbb{R}^{3\times 3}$ is the system inertial matrix, reported in Eq. (4). $\boldsymbol{D} \in \mathbb{R}^{3\times 3}$ is the matrix representing the linear hydrodynamic damping forces and moments, as reported in Eq. (5).

$$\boldsymbol{J}(\boldsymbol{\tau}) = \begin{bmatrix} \cos(\psi) & -\sin(\psi) & 0 \\ \sin(\psi) & \cos(\psi) & 0 \\ 0 & 0 & 1 \end{bmatrix}, \tag{3}$$

$$\boldsymbol{M} = \begin{bmatrix} \Delta - X_{\dot{u}} & 0 & 0 \\ 0 & \Delta - Y_{\dot{v}} & \Delta x_G - Y_{\dot{y}} \\ 0 & \Delta x_G - N_{\dot{v}} & I_z N_{\dot{y}} \end{bmatrix}, \tag{4}$$

$$\boldsymbol{D} = \begin{bmatrix} -X_u & 0 & 0 \\ 0 & -Y_v & -Y_y \\ 0 & -N_v & -N_y \end{bmatrix}. \tag{5}$$

$X_{\dot{u}}$, $Y_{\dot{v}}$, $Y_{\dot{y}}$, $N_{\dot{v}}$, $N_{\dot{y}}$ are the added mass forces for surge, sway, and yaw DOFs. I_z is the Z-axis' component of the moment of inertial about the body-fixed reference frame. x_G is the distance between the center of gravity and the origin of the body-fixed reference frame. Given the lack of detailed information regarding the geometry of the case study under consideration, we approximated their values using the method proposed in [61].

C. Environmental Disturbances

As described in Section II-B, the environmental disturbances acting on the vessel include waves, wind and current forces. We adopt a feed-forward model for all of them, and assume that the total environmental forces acting on the vessel are the superposition of these three effects.

1) Wind Forces: The wind forces acting on the vessel are proportional to the projected area above the waterline and the square of the wind speed, relative to the vessel. The norm of the relative wind speed is defined as:

$$V_{rw} = \sqrt{u_{rw}^2 + w_{rw}^2}, \tag{6}$$

where $u_{rw} = u - V_w \cos(\gamma_{rw})$ and $w_{rw} = w - V_w \sin(\gamma_{rw})$ are the wind speed components, V_w is the sustained wind velocity $10m$ above the sea, $\gamma_{rw} = \gamma_w - \psi$ is the relative wind angle on the body-fixed reference frame, and γ_w is the wind direction. The wind loads can be formulated as follows [1]

$$\boldsymbol{f_w} = \frac{1}{2}\rho_a V_{rw}^2 \begin{bmatrix} C_{wx}(\gamma_{rw}) A_{Fw} \\ C_{wy}(\gamma_{rw}) A_{Lw} \\ C_{wn}(\gamma_{rw}) L_{oa} \end{bmatrix}, \tag{7}$$

where ρ_a is the air density and A_{Fw} and A_{Lw} are the frontal and lateral projected areas of the non-submerged part of the vessel projected on the xz- and yz-planes respectively. C_{wx}, C_{wy}, C_{wn} are the adimensional wind drag coefficients in surge, sway, and yaw directions computed according to [62].

2) Current Forces: We have assumed irrotational and constant currents, whose effects in surge and sway motions were modelled as follows [1]

$$\boldsymbol{v_c} = \begin{bmatrix} u_c \\ w_c \end{bmatrix} = \begin{bmatrix} V_c \cos(\gamma_c) \\ V_c \sin(\gamma_c) \end{bmatrix}. \tag{8}$$

The norm of the relative current velocity is defined as

$$V_{rc} = \sqrt{u_{rc}^2 + w_{rc}^2}, \tag{9}$$

where $u_{rc} = u - u_c$ and $w_{rc} = w - w_c$ are the relative current velocities in the surge and sway motions respectively.

Finally, by defining the current direction relative to the vessel heading as $\gamma_{rc} = \gamma_c - \psi$, we can estimate the static current loads as follows [62]

$$\boldsymbol{f_c} = \frac{1}{2}\rho_w V_{rc}^2 \begin{bmatrix} C_{cx}(\gamma_{rc}) L_{pp} T \\ C_{cy}(\gamma_{rc}) L_{pp} T \\ C_{cn}(\gamma_{rc}) L_{pp}^2 T \end{bmatrix}, \tag{10}$$

where ρ_w is the density of the water, C_{cx}, C_{cy}, C_{cn} are the current drag coefficients in surge, sway, and yaw, and L_{pp}, T are the length between perpendiculars and draft of the vessel We estimated those from empirical formulas [62], as functions of the main dimensions of the vessel.

3) Wave Forces: As stated at the beginning of this section, we assume that wave filtering techniques have been successfully employed. This allows us to neglect the first-order wave-induced forces and focus only on the wave drift forces, namely non-zero slowly varying components. Common practice is to solve the first-order problem using potential flow theory [63]. The mean drift forces can be obtained by applying the theory of conservation of momentum, namely the far-field theory. In this work, we employed the ShipX software [64] to obtain the mean drift coefficients $C_{wav,x}$, $C_{wav,y}$, $C_{wav,n}$. Hence, the mean wave drift forces follow from [63]

$$\boldsymbol{f_{wav}} = \begin{bmatrix} C_{wav,x} H_s^2 \cos(\gamma_{wav} - \psi) \\ C_{wav,y} H_s^2 \sin(\gamma_{wav} - \psi) \\ C_{wav,n} H_s^2 \sin\left(2\left(\gamma_{wav} - \psi\right)\right) \end{bmatrix}, \tag{11}$$

where H_s is the significant wave height and γ_w is the wave angle on the fixed body reference frame.

D. Azimuth Thrusters

As shown in Figure 3, the vessel is equipped with $k_p = 6$ azimuth thrusters. We take into account the actuators' force vector as follows

$$\boldsymbol{f} = \boldsymbol{T_{t,e}} \boldsymbol{K_{t,e}} \boldsymbol{u_{t,e}}. \tag{12}$$

$\boldsymbol{T_{t,e}} \in \mathbb{R}^{3\times 2k_p}$ (see Eq. (13)) is the extended thrust configuration vector, $\boldsymbol{K_{t,e}} \in \mathbb{R}^{2k_p \times 2k_p}$ (see Eq. (14)) is the diagonal force coefficient matrix, and $\boldsymbol{u_{t,e}} \in \mathbb{R}^{2k_p \times 1}$ (see Eq. (15)) is the vector of extended control inputs of the thrusters

$$\boldsymbol{T_{t,e}} = \begin{bmatrix} 1 & 0 & & 1 & 0 \\ 0 & 1 & \dots & 0 & 1 \\ -h_{y,1} & h_{x,1} & & -h_{y,6} & h_{x,6} \end{bmatrix}, \tag{13}$$

$$\boldsymbol{K_{t,e}} = \text{diag}\left\{k_1, k_1, \cdots, k_6, k_6\right\}, \tag{14}$$

$$\boldsymbol{u_{t,e}} = \begin{bmatrix} u_{1,x} & u_{1,y} & \cdots & u_{6,x} & u_{6,y} \end{bmatrix}^\intercal, \tag{15}$$

where $h_{x,i}$, $h_{y,i}$ are the moment arms and $u_{x,i} = u_i \cos(\alpha_i)$ and $u_{y,i} = u_i \sin(\alpha_i)$ refer to the normalised thrust of each thruster in the longitudinal and lateral directions. Consequently, we can define the norm of the extended thrust vector $\boldsymbol{u_t} \in \mathbb{R}^{k_p \times 1}$ and the azimuth angle vector $\boldsymbol{a} \in \mathbb{R}^{k_p \times 1}$ as

$$u_{t,i} = \sqrt{u_{x,i}^2 + u_{y,i}^2}, \tag{16}$$

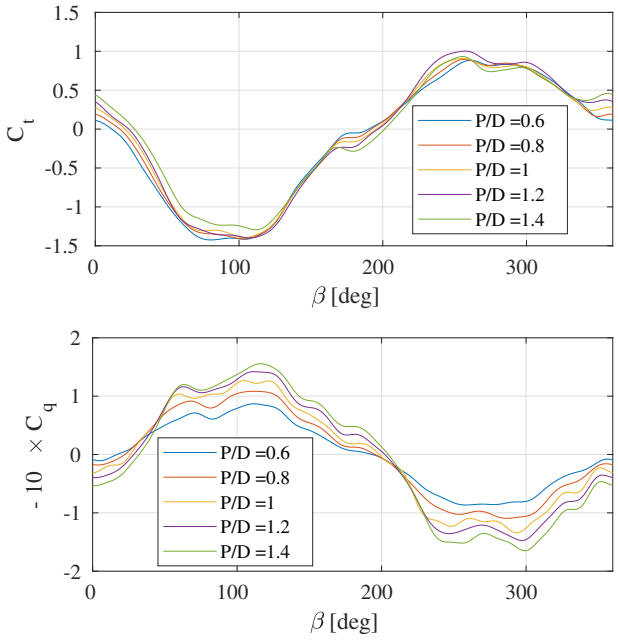

Figure 4: Four-quadrant open water diagram of the ducted propellers from the Maritime Research Institute Netherlands [65].

$$\boldsymbol{a} = \arctan\left(\boldsymbol{u_y} \oslash \boldsymbol{u_x}\right), \tag{17}$$

where $\oslash$ indicates element-wise division.

Since thrusters are identical, the diagonal elements of the matrix $\boldsymbol{K_e}$ are equal to

$$k_i = \frac{T_{p,max}}{0.5\rho_w \left(V_S^2 + \left(0.7\pi n_{p,i} D_p\right)^2\right) \pi \frac{D_p^2}{4}}, \tag{18}$$

$$V_S = \sqrt{u^2 + w^2}, \tag{19}$$

where $T_{p,max}$ and $n_{p,i}$ are the maximum thrust force and rotational speed of each thruster, D_p is the propeller diameter, and V_S is the norm of the vessel speed.

In this work, as a novel contribution, we generalise the traditional control approaches that consider either fixed-speed CPPs or variable-speed FPPs [2]. For this reason we need to be able to predict the propellers' thrust and torque characteristics based on the propeller pitch vector $\boldsymbol{u_p} \in \mathbb{R}^{k_p \times 1}$ and the rotational speed vector $\boldsymbol{n_p} \in \mathbb{R}^{k_p \times 1}$. To this end, we made use of the the four-quadrant open water diagram of the ducted propellers from the Maritime Research Institute Netherlands [65], shown in Figure 4, which describes the relationship between the hydrodynamic pitch angle vector $\boldsymbol{\beta} \in \mathbb{R}^{k_p \times 1}$ and the non-dimensional thrust and torque $\boldsymbol{C_t}$, $\boldsymbol{C_q} \in \mathbb{R}^{k_p \times 1}$ coefficients.

Subsequently, we can establish a relationship between the norm of the propeller thrust and the rotational speed vectors in order to derive the norm of the torque vector $\boldsymbol{M_p} \in \mathbb{R}^{k_p \times 1}$ as follows

$$\boldsymbol{\beta} = \arctan\left(\frac{u_a}{0.7\pi \boldsymbol{n_p} D_p}\right), \tag{20}$$

$$u_a = (1 - f_w) V_S, \tag{21}$$

$$\boldsymbol{C_t} = \boldsymbol{u_t} \oslash \left(u_a^2 + \left(0.7\ \pi\ D_p\ \boldsymbol{n_p}\right)^{\circ 2}\right) \frac{T_{p,\max}(1 - f_t)}{\frac{\pi \rho_w}{8} D_p^2}, \tag{22}$$

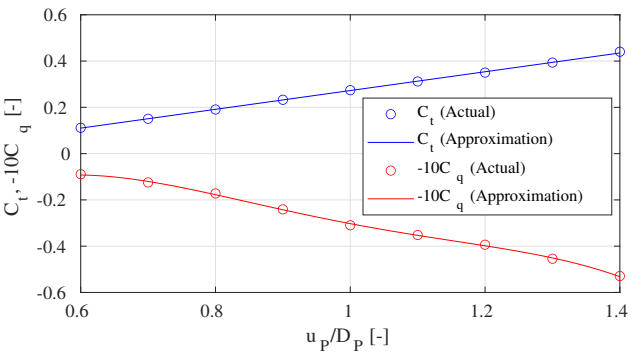

Figure 5: Approximation of the propeller thrust and torque coefficients by means of Eqns. (25)-(26).

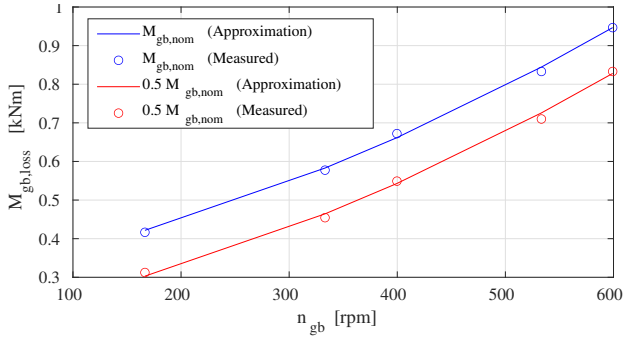

Figure 6: Approximation of the gearbox losses by means of Eq. (32) at various operating conditions.

$$\boldsymbol{C_q} = \boldsymbol{M_p} \oslash \left(u_a^2 + (0.7\ \pi\ D_p\ \boldsymbol{n_p})^{\circ 2}\right) \frac{\eta_r}{\frac{\pi \rho_w}{8} D_p^3}, \tag{23}$$

where f_w, f_t, η_r are the wake factor, the thrust deduction factor, and the relative rotative efficiency of each propeller. It is worth noting that we assumed those quantities as constant for all the operating conditions and across all the propellers. We can also define the delivered power vector of the thrusters as follows

$$\boldsymbol{P_p} = 2\pi \boldsymbol{n_p} \circ \boldsymbol{M_p}, \tag{24}$$

where $\circ$ indicates element-wise multiplication.

When the vessel is in stationary position during DP operations, it is possible to assume that $v_a \approx 0$. Under this assumption, the torque coefficient of Eq. (23) can be expressed as a third degree polynomial taking into account propeller pitch for a near-zero hydrodynamic pitch angle

$$\tilde{\boldsymbol{C}}_{\boldsymbol{q}} \approx \sum_{i=0}^{3} c_{q_0,i} \frac{\boldsymbol{u_p}^{\circ i}}{D_p^i}. \tag{25}$$

Analogously, we can approximate also the thrust coefficient as follows

$$\tilde{\boldsymbol{C}}_t \approx \sum_{i=0}^{1} c_{t_0,i} \frac{\boldsymbol{u_p}^{\circ i}}{D_p^i}. \tag{26}$$

The quality of these approximations can be verified by means of Figure 5. By means of these approximations, we can easily express the propellers' rotational speed and torque on the basis of the thrust and pitch vectors

$$\boldsymbol{C_q} = \tilde{\boldsymbol{C}}_{\boldsymbol{q}} \Rightarrow$$
$$\boldsymbol{M_p} = \frac{\pi \rho_w}{8} \frac{D_p^3}{\eta_r} \sum_{i=0}^{3} \left(c_{q_0,i} \frac{\boldsymbol{u_p}^{\circ i}}{D_p^i} \right) \circ (0.7\ \pi\ D_p\ \boldsymbol{n_p})^{\circ 2}, \tag{27}$$
$$\boldsymbol{C_t} = \tilde{\boldsymbol{C}}_{\boldsymbol{t}} \Rightarrow$$
$$\boldsymbol{n_p} = \frac{((1-f_t)T_{p,max})^{\frac{1}{2}}}{(0.7\pi D_p)^2 \left(\frac{\pi \rho_w}{8} D_p^2\right)^{\frac{1}{2}}} \left(\boldsymbol{u_t} \oslash \sum_{i=0}^{1} c_{t_0,i} \frac{\boldsymbol{u_p}^{\circ i}}{D_p^i} \right)^{\circ \frac{1}{2}}. \tag{28}$$

E. Gearbox and shaft-line

Literature related to the modelling and simulation of maritime Gearboxes (gb) is rather limited, even though, lately, this subject has received increasingly attentions due to novel numerical modelling methods [66]. Overall, approaches consist of either complex thermal network models [67] or simple GB loss functions, as those presented in [68], [69]. While the thermal network models are usually based on adimensional heuristic estimation models for the various loss sources, they unfortunately require very detailed design information of the gearbox, which is usually not readily available in real world applications. However, the authors of [67] demonstrated that a properly calibrated empirical model can accurately match the predictions of a much more detailed thermal network model. In this work, we have exploited the quadratic model for the GB losses proposed in [70] and a linear model for the losses on the shaft bearings as functions of rotational speed and torque

$$\boldsymbol{M_{sh}} = \boldsymbol{M_p} + \boldsymbol{M_{sh,loss}}, \tag{29}$$
$$\boldsymbol{M_{sh,loss}} = c_{sh,1} + c_{sh,2}\boldsymbol{n_p} + c_{sh,3}\boldsymbol{M_{sh}}, \tag{30}$$
$$\boldsymbol{M_{gb}} = \boldsymbol{M_{sh}} + \boldsymbol{M_{gb,loss}}, \tag{31}$$
$$\boldsymbol{M_{gb,loss}} = c_{gb,1} + c_{gb,2}\boldsymbol{n_{em}} + c_{gb,3}\boldsymbol{n_{em}}^{\circ 2} + c_{gb,4}\boldsymbol{M_{gb}}, \tag{32}$$

where $\boldsymbol{M_{sh}}$, $\boldsymbol{M_{sh,loss}} \in \mathbb{R}^{k_p \times 1}$ are the normalised shaft torque and torque loss vectors, $\boldsymbol{M_{gb}}$ and $\boldsymbol{M_{gb,loss}} \in \mathbb{R}^{k_p \times 1}$ are the normalised GB torque and torque loss vectors and the set of scalars $c_{sh,i}$, and $c_{gb,i}$ are the fitted loss coefficients, obtained by Least Squares Errors (LSE) estimation. The empirical model for the GB losses is parameterised using the set of on-board measurements from the marine GB presented in [69] under several steady-state operating conditions. Figure 6 shows the quality of the approximations.

F. Electric Motors

For the purpose of this work, it is necessary to accurately assess the losses of the asynchronous Electric Motors (EMs) at various operating conditions in terms of rotational speed and torque. Unfortunately, manufacturers only report the nominal efficiency. Consequently, in order to assess the losses of the asynchronous EMs, we employed the fifth-order state-space model according defined in [71], [72] and we obtained the efficiency map $\boldsymbol{\eta_{em}} \in \mathbb{R}^{k_p \times 1}$. We have assumed balanced supply voltage, thus neglecting the zero sequence current. For each electric motor, the model is defined as follows

$$\begin{bmatrix} v_{qs} & v_{ds} & v'_{qr} & v'_{dr} \end{bmatrix}^T = \tag{33}$$

$$\begin{bmatrix} r_s+\frac{q}{\omega_b}l_{ss} & -\frac{\omega_e}{\omega_b}l_{ss} & 0 & \frac{q}{\omega_b}l_M & \frac{\omega_e}{\omega_b}l_M & 0 \\ -\frac{\omega}{\omega_b}l_{ss} & r_s+\frac{q}{\omega_b}l_{ss} & 0 & -\frac{\omega_e}{\omega_b}l_M & \frac{p}{\omega_b}l_M & 0 \\ \frac{p}{\omega_b}l_M & \omega_{eq}l_M & 0 & r'_r+\frac{q}{\omega_b}l'_{rr} & \omega_{eq}l_{rr} & 0 \\ -\omega_{eq}l_M & \frac{p}{\omega_b}l_M & 0 & -\omega_{eq}l'_{rr} & r'_r+\frac{q}{\omega_b}l'_{rr} & 0 \end{bmatrix} \begin{bmatrix} i_{qs} \\ i_{ds} \\ i'_{qr} \\ i'_{dr} \end{bmatrix},$$

$$\begin{bmatrix} \psi_{qs} \\ \psi_{ds} \\ \psi'_{qr} \\ \psi'_{dr} \end{bmatrix} = \begin{bmatrix} l_{ss} & 0 & 0 & l_M & 0 & 0 \\ 0 & l_{ss} & 0 & 0 & l_M & 0 \\ l_M & 0 & 0 & l'_{rr} & 0 & 0 \\ 0 & l_M & 0 & 0 & l'_{rr} & 0 \end{bmatrix} \begin{bmatrix} i_{qs} \\ i_{ds} \\ i'_{qr} \\ i'_{dr} \end{bmatrix}, \tag{34}$$

$$l_{ss} = l_{ls} + l_M, \tag{35}$$

$$l'_{rr} = l'_{lr} + l_M, \tag{36}$$

$$M_{em} = \frac{3}{2}\frac{q}{2}\frac{1}{\omega_b}\left(\psi'_{qr}i'_{dr} - \psi'_{dr}i'_{qr}\right), \tag{37}$$

$$\omega_{eq} = \frac{\omega_e - \omega_r}{\omega_b}, \tag{38}$$

$$\omega_e = \omega_r - \omega_b\frac{r'_r i'_{qr}}{\psi'_{dr}}, \tag{39}$$

$$\omega_r = \omega_{em}q = 2\pi q n_{em}. \tag{40}$$

$i_{dq,rs}$, $v_{dq,rs}$, $\psi_{dq,rs}$ are the direct and quadrature currents, voltages, and flux linkages in the rotor and stator. r_s, r'_r and l_s, l'_r are the stator and rotor resistances and inductances. l_M is the mutual inductance. q is the number of poles of the induction motor. All these parameters were obtained from EMs of similar size and plate data available in the literature [69]. Also, ω_b, ω_e, ω_r, and ω_{em} are the base, rotating reference frame, electric rotor, and EM shaft frequencies.

Furthermore, we assume that the EMs are controlled with direct field oriented control, as proposed by [73] and discussed in depth in [71], [74]. The quadrature and direct current references ($i_{ds,set}$, $i_{qs,set}$), in the synchronously rotating reference frame, are determined from the torque and direct rotor flux references. The measured quadrature and direct currents are determined as follows

$$\begin{bmatrix} i_{qs,set} \\ i_{ds,set} \end{bmatrix} = \begin{bmatrix} \frac{M_{em}}{\frac{3}{2}\frac{q}{2}\frac{l_M}{l'_{rr}}\frac{\psi'_{dr}}{\omega_b}} \\ \frac{\psi'_{dr}}{\omega_b}\left(r'_r + l'_{rr}\right)\frac{1}{r_r l_M} \end{bmatrix} + \begin{bmatrix} i_{qs} \\ i_{ds} \end{bmatrix}. \tag{41}$$

Subsequently, PID control is applied in order to obtain the voltage reference vector $\boldsymbol{v_{ref}} = [v_{ds,ref}, v_{qs,ref}]$ with an extra feed-forward term to obtain the final quadrature and direct voltage references $\boldsymbol{v_{set}} = [v_{ds,set}, v_{qs,set}]$ as follows

$$\boldsymbol{v_{set}} = \boldsymbol{K_u}\boldsymbol{I_u} + \boldsymbol{v_{ref}}, \tag{42}$$

$$\boldsymbol{K_u} = \begin{bmatrix} \frac{l_M^2}{l'_{rr}} & -\omega_{mf}\frac{l'_{lr}}{l_m}l_{ss} \\ \omega_{mf}\frac{l'_{lr}}{l_M}l_{ss} & \frac{l_M^2}{l'_{rr}} \end{bmatrix}, \tag{43}$$

$$\boldsymbol{I_u} = \begin{bmatrix} \frac{\partial i_{ds,set}}{\partial t} & i_{d,s,set} \\ i_{qs,set} & \frac{\partial i_{qs,set}}{\partial t} \end{bmatrix}, \tag{44}$$

$$\omega_{mf} = \omega_e + \omega_{sl}, \tag{45}$$

$$\omega_{sl} = r'_r\frac{l_M}{l'_{rr}}\frac{i_{qs,set} - i_{qs}}{\psi_{dr,set}}\omega_b, \tag{46}$$

where ω_{sl} and ω_{mf} are the slip and magnetic field angular speeds.

The efficiency map obtained from the state-space model was then approximated by means of the Willans approach [75] as follows

$$\boldsymbol{\eta_{em}} = (c_{em,0}\boldsymbol{n_{em}}\circ\boldsymbol{M_{em}}) \oslash (\boldsymbol{n_{em}}\circ\boldsymbol{M_{em}} + c_{em,1}), \tag{47}$$

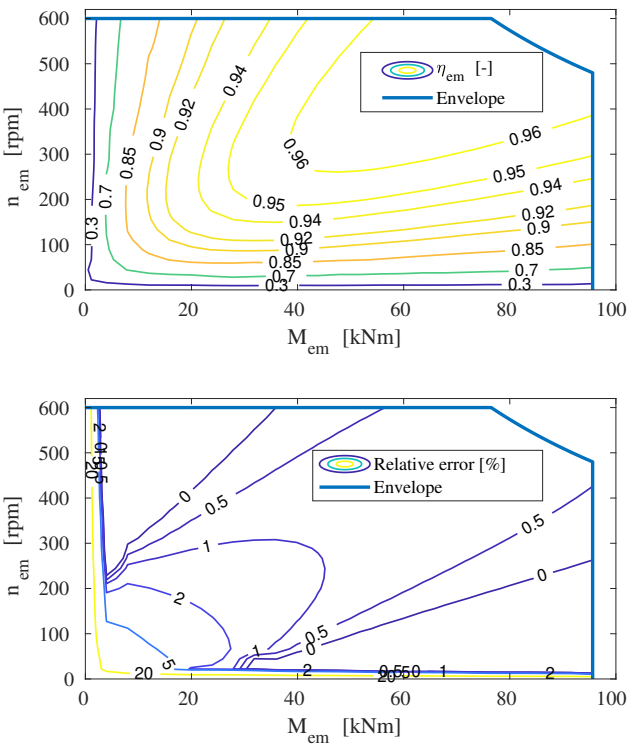

Figure 7: Electric motor efficiency map (top) and approximation errors (bottom) by means of Eq. (47).

$$\boldsymbol{n_{em}} = i_{gb}\boldsymbol{n_p}, \tag{48}$$

$$\boldsymbol{M_{em}} = \boldsymbol{M_p} + \boldsymbol{M_{sh,loss}} + \boldsymbol{M_{gb,loss}} \tag{49}$$

where $\boldsymbol{n_{em}}$ is the rotational speed of the EM, i_{gb} is the reduction ratio of the identical GBs, $\boldsymbol{M_{em}} \in \mathbb{R}^{k_p \times 1}$ refers to the normalised torque of the EM, and $c_{em,i}$ are approximation constants obtained through LSE.

The approximation errors between the state-space model and the Willans approach are presented in Figure 7. Considering a grid of 25 equidistant points along each dimension (n_{em}, M_{em}) of the efficiency map, the error of the model is around 4%. However, Figure 7 indicates that the errors are different depending on the zone. We can see that the error for most of the operating zones is less than 2%, however in the near-zero speed and torque regions, the error is around 20%. This can be seen as a weakness, but, for the purpose of this work, it turns out to generate a positive side effect. In fact, in the zones where the efficiency of the electric motor is low ($\leq 30\%$ according to the state-space model) our approximation underestimates the efficiency even further. This provides an extra incentive to the optimisation algorithm to avoid these operating conditions for the EMs.

G. Frequency Converters

Since we are investigating the fuel savings potential, we do not need to study the dynamics of the electrical network. In fact, the time constant of the electrical systems is at least one order of magnitude smaller than the mechanical one. Consequently, transient operation does not have a significant effect on the overall fuel consumption. Moreover, we can safely assume that the induction motors are fed by an ideal

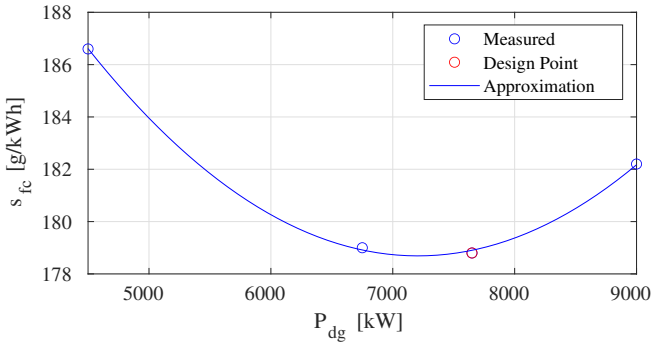

Figure 8: Approximation of the Diesel-generator specific fuel consumption by means of Eq. (50).

voltage source [76]. Hence, frequency converters are modelled as ideal voltage sources providing the requested voltage and frequency to the EMs.

H. Diesel Generators

We estimate the instantaneous fuel consumption of the DGs by means of a quadratic relation between torque and injected fuel per cycle, as proposed by [77], [78]. The auxiliary DGs, namely DGs exploited for the on-board electrical power generation, are usually operated at the nominal fixed speed to optimise their efficiency. Hence, we will omit the dependency on engine speed, since it is constant, and we can directly link the specific fuel consumption vector of the DGs $\boldsymbol{s_{fc}} \in \mathbb{R}^{k_{dg}\times 1}$ to the control vector $\boldsymbol{u_{dg}} \in \mathbb{R}^{k_{dg}\times 1}$ as follows

$$\boldsymbol{s_{fc}} = \boldsymbol{z_{dg}} \circ \sum_{i=0}^{2} c_{dg,i} \boldsymbol{u_{dg}}^{\circ i}. \tag{50}$$

$\boldsymbol{z_{dg}} \in \mathbb{R}^{k_{dg}\times 1}$ is the vector of binary variables indicating if each DG is connected to the grid. k_{dg} is the number of DGs on the system. $c_{dg,i}$ are scalar values derived by means of LSE and constant across all DGs, since they are identical. The quality of this approximation can by appreciated in Figure 8. Finally, the total fuel consumption of the DP system $(\dot{m}_{f_{tot}})$ can be expressed as the sum of the fuel consumption among all DGs

$$\dot{m}_f = \boldsymbol{u_{dg}}^{\mathsf{T}} \boldsymbol{s_{fc}} \tag{51}$$

III. Formulating and Solving the Thrust Allocation Problem

The control system needs to solve the so called thrust allocation problem, in order to ensure the vessels' position and heading using its own thrusters to compensate exogenous disturbances. This requires the development of a Thrust Allocation algorithm able to contemporary maintain the vessel position and heading while minimising the fuel consumption. The resulting thrust allocation optimisation problem can be sketched as follows

$$\begin{aligned} \min_{\boldsymbol{u}} \quad & f(\boldsymbol{u}, \boldsymbol{w}) \\ \text{s.t.} \quad & \boldsymbol{h}(\boldsymbol{u}, \boldsymbol{w}) = 0, \ \boldsymbol{g}(\boldsymbol{u}, \boldsymbol{w}) \leq 0, \end{aligned}$$

where $\boldsymbol{u} = [\boldsymbol{u_{t,e}}, \boldsymbol{u_p}, \boldsymbol{u_{dg}}, \boldsymbol{z_{dg}}]^{\mathsf{T}}$ is the combined control vector, $\boldsymbol{w} = [V_w, V_c, V_{wav}, \gamma_w, \gamma_c, \gamma_{wav}]^{\mathsf{T}}$ is the exogenous inputs vector, $f(\boldsymbol{u}, \boldsymbol{w})$ is the objective function to be minimised (the fuel consumption), and $\boldsymbol{h}(\boldsymbol{u}, \boldsymbol{w})$ and $\boldsymbol{g}(\boldsymbol{u}, \boldsymbol{w})$ are the equality (e.g. keep the vessel position and heading) and inequality constraint (e.g. operational limitation) vectors. Furthermore, in this work, we will study and manipulate this optimisation problem in such a way that it will be possible to solve it in near-real time on conventional on-board computing platforms.

In the next sections we will present the complete, detailed, and complex thrust allocation optimisation problem leveraging on the notions described in Section II. We will quantify the extra savings in fuel consumption with respect to the more conventional modelisation approaches adopted in literature (e.g. minimisation of the propeller power or the total thrust). Furthermore, in order to reduce the computational requirement and be able to adopt the proposal in near-real time control, we will exploit reasonable and theoretical proprietaries.

A. Constraints

The first set of constraints are the boundaries for the decision variables, namely the pitch, the thrust, and diesel-generator power set-points, which represent the pre-defined manufacturer limits

$$p_{\min} \leq \boldsymbol{u_p} \leq p_{\max}, \tag{52}$$

$$0 \leq \boldsymbol{u_{dg}} \leq P_{dg,\max}, \tag{53}$$

$$\boldsymbol{z_{dg}} \in \mathbb{Z}_2. \tag{54}$$

Then, we have to take into account other kinds of constraints. In particular, we have to counteract the environmental disturbances, to balance the propulsive power supply and demand, and to satisfy the operating limits of all the components of the DP system. For this purpose, we define the constraints that limit the maximum thrust that can be delivered by each thruster

$$0 \leq \left(\boldsymbol{u_x}^{\circ 2} + \boldsymbol{u_y}^{\circ 2}\right)^{\circ \frac{1}{2}} \leq T_{p,max}. \tag{55}$$

Since the 3-DOF kinematic model has been employed in this work, the DP system must counteract the environmental disturbances in the surge, sway, and yaw motions

$$\boldsymbol{T_{t,e}} \boldsymbol{K_{t,e}} \boldsymbol{u_{t,e}} = \boldsymbol{f_{wav}} + \boldsymbol{f_c} + \boldsymbol{f_w} = \boldsymbol{f_{env}}. \tag{56}$$

Leveraging on Eqns. (7), (10), (11), (13)-(16) we can express the equality constraints on the basis of the control vector $\boldsymbol{u_t}$ and the exogenous inputs $\boldsymbol{w}$

$$\begin{bmatrix} \sum_{i=1}^{k_p} u_{x,i} \\ \sum_{i=1}^{k_p} u_{y,i} \\ \sum_{i=1}^{k_p} h_{y,i} u_{x,i} - h_{x,i} u_{y,i} \end{bmatrix} = \frac{1}{\sigma_1} \begin{bmatrix} F_{env,u} \\ F_{env,v} \\ F_{env,y} \end{bmatrix}, \tag{57}$$

where

$$\sigma_1 = \frac{(1-f_t) T_{p,max}^2}{(0.7\pi D_p)^2 \left(\frac{\pi \rho_w}{8} D_p^2\right)^2}. \tag{58}$$

The balance between power supply and demand can be formulated as a power balance across the main Switchboard (SB). Under the assumption of an ideal SB [76], the power required from the EMs to counteract the environmental disturbances must be equal to the power provided by the DGs

$$\sum_{i=1}^{k_{dg}} u_{dg,i} = \sum_{i=1}^{k_{em}} 2\pi n_{em,i} M_{em,i} \frac{1}{\eta_{em,i}} \tag{59}$$

By means of a series of technical steps, exploiting Eqns. (27) and (28) in Eqns.(29)-(49) and Eqns.(47)-(48), it is possible to express the power balance in terms of the control vectors $\boldsymbol{u_p}, \boldsymbol{u_t}, \boldsymbol{u_{dg}}$

$$\sum_{i=1}^{k_{dg}} u_{dg,i} = \sum_{i=1}^{k_{em}} \sigma_2 + \sigma_3 \left(\frac{\left(u_{x,i}^2 + u_{y,i}^2\right)^{\frac{1}{2}}}{\sum_{j=0}^{1} c_{t_0,j} \frac{u_{p,i}^j}{D_p^j}} \right)^{\frac{1}{2}} + \\ + \sigma_4 \frac{\left(u_{x,i}^2 + u_{y,i}^2\right)^{\frac{1}{2}}}{\sum_{j=0}^{1} c_{t_0,j} \frac{u_{p,i}^j}{D_p^j}} + \sigma_5 \left(\frac{\left(u_{x,i}^2 + u_{y,i}^2\right)^{\frac{1}{2}}}{\sum_{j=0}^{1} c_{t_0,j} \frac{u_{p,i}^j}{D_p^j}} \right)^{\frac{3}{2}} + \\ + \sigma_6 \frac{\left(u_{x,i}^2 + u_{y,i}^2\right)^{\frac{3}{4}}}{\left(\sum_{j=0}^{1} c_{t_0,j} \frac{u_{p,i}^j}{D_p^j}\right)^{\frac{1}{2}}}, \tag{60}$$

$$\sigma_2 = \frac{c_{em,1}}{c_{em,0}}, \tag{61}$$

$$\sigma_3 = \frac{2\pi}{c_{em,0}} \frac{\left((1-f_t)T_{p,max}\right)^{\frac{1}{2}}}{\left(0.7\pi D_p\right)^2 \left(\frac{\pi\rho_w}{8} D_p^2\right)^{\frac{1}{2}}} \\ \left(c_{sh,1} \left(1 + \frac{c_{sh,3}}{1-c_{sh,3}}\right) + \frac{c_{gb,4}}{1-c_{gb,4}} \frac{c_{sh,1}+c_{sh,2}}{1-c_{sh,3}} + c_{gb,1} \right), \tag{62}$$

$$\sigma_4 = \frac{2\pi}{c_{em,0}} \frac{(1-f_t)T_{p,max}}{\left(0.7\pi D_p\right)^4 \left(\frac{\pi\rho_w}{8} D_p^2\right)} \\ \left(c_{sh,2} \left(1 + \frac{c_{sh,3}}{1-c_{sh,3}}\right) + \right. \\ \left. + \frac{c_{gb4}}{1-c_{gb,4}} \left(\frac{c_{sh,2}}{1-c_{sh,3}} + c_{gb,2} i_{gb} \right) + c_{gb,2} i_{gb} \right), \tag{63}$$

$$\sigma_5 = \frac{2\pi}{c_{em,0}} \frac{\left((1-f_t)T_{p,max}\right)^{\frac{3}{2}}}{\left(0.7\pi D_p\right)^6 \left(\frac{\pi\rho_w}{8} D_p^2\right)^{\frac{3}{2}}} \\ \left(1 + \frac{c_{gb,4}}{1-c_{gb,4}}\right) c_{gb,3} i_{gb}^2, \tag{64}$$

$$\sigma_6 = \frac{2\pi}{c_{em,0}\eta_r} \frac{\left((1-f_t)T_{p,max}\right)^{\frac{3}{2}}}{\left(0.7\pi D_p\right)^4 \left(\frac{\pi\rho_w}{8} D_p^2\right)^{\frac{1}{2}}} \\ \left(1 + \frac{c_{gb,4}}{1-c_{gb,4}} + \frac{1}{1-c_{sh,3}} \left(c_{sh,3}+1\right)\right). \tag{65}$$

Closely-placed azimuth thrusters exhibit a decrease in efficiency when they operate in the wake stream of each other [3]. In order to avoid these adverse interaction effects, forbidden zones for some azimuth angles must be defined. Using the Dynamic Positioning System guide (DPS) of the American Bureau of Shipping [79], we were able to define the forbidden zones on the basis of the relative positions of the thrusters and the propeller diameter. To this end, we have defined the feasible regions for all thrusters to lie between predefined azimuth angle ranges $\boldsymbol{\alpha_{min}}, \boldsymbol{\alpha_{max}} \in \mathbb{R}^{k_p \times 1}$

$$\boldsymbol{\alpha_{min}} \leq \arctan\left(\boldsymbol{u_y} \oslash \boldsymbol{u_x}\right) \leq \boldsymbol{\alpha_{max}}. \tag{66}$$

We have shown these regions also in Figure 9.

Constraints on the torque output of the EMs are also necessary, to prevent operations outside the predefined manufacturer limits

$$0 \leq \boldsymbol{M_{em}} \leq M_{\text{em,max}}. \tag{67}$$

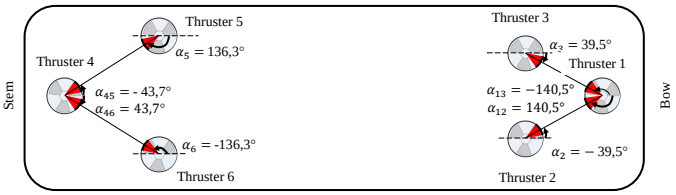

Figure 9: Azimuth thrusters forbidden zones.

We can express these constraints on the basis of the control vectors $\boldsymbol{u_t}$, $\boldsymbol{u_p}$ by means of Eqns. (23), (27), and (29)-(49)

$$0 \leq \sigma_7 + \left(\frac{D_p}{\eta_r} \sum_{i=0}^{3} c_{q_0,i} \frac{\boldsymbol{u_p}^{\circ i}}{D_p^i} + \sigma_8 \right) \circ \sigma_9 \boldsymbol{g} + \sigma_{10} \left(\boldsymbol{g}\right)^{\circ \frac{1}{2}} \leq M_{\text{em,max}},$$

$$\boldsymbol{g} = \left(\boldsymbol{u_x}^{\circ 2} + \boldsymbol{u_y}^{\circ 2}\right)^{\circ \frac{1}{2}} \oslash \sum_{i=0}^{1} c_{t_0,i} \frac{\boldsymbol{u_p}^{\circ i}}{D_p^i}. \tag{68}$$

$M_{\text{em,max}}$ is the maximum admissible torque output of the identical EMs. σ_i can be expressed as follows

$$\sigma_7 = \frac{1}{1-c_{sh,3}} \left(c_{sh,1} - \frac{c_{gb,1}}{c_{gb,4} - i_{gb}} \right), \tag{69}$$

$$\sigma_8 = \frac{1}{1-c_{sh,3}} \frac{8 c_{gb,3} {i_{gb}}^2}{0.7^2 \pi^3 \rho {D_p}^4}, \tag{70}$$

$$\sigma_9 = \frac{1}{1-c_{sh,3}} \frac{1-f_t}{c_{gb,4} - i_{gb}}, \tag{71}$$

$$\sigma_{10} = \frac{1}{1-c_{sh,3}} \frac{2\sqrt{2} i_{gb}}{0.7\pi D_p} \left(\frac{c_{gb,2}}{c_{gb,4} - i_{gb}} + c_{sh,2} \right) \left(\frac{1-f_t}{\pi \rho_w D_p^2} \right)^{\frac{1}{2}}. \tag{72}$$

The rotational speed of each propeller and electric motor must satisfy the manufacturers limitations

$$0 \leq \boldsymbol{n_p} \leq n_{p_{max}}, \tag{73}$$

$$0 \leq \boldsymbol{n_{em}} \leq n_{em_{max}}. \tag{74}$$

We can combine the two constraints reported in Eqns. (73) and (74) and express them in terms of the control vectors $\boldsymbol{u_t}, \boldsymbol{u_p}$ using Eqns. (28) and (48)

$$0 \leq \left(\boldsymbol{u_x}^{\circ 2} + \boldsymbol{u_y}^{\circ 2}\right)^{\circ \frac{1}{2}} \oslash \sum_{i=0}^{1} c_{t_0,i} \frac{\boldsymbol{u_p}^{\circ i}}{D_p^i} \leq \sigma_{11}. \tag{75}$$

Note that

$$\sigma_{11} = \\ \min\left(n_{p,max}, \frac{n_{em,max}}{i_{gb}} \right) \left(\frac{1}{0.7\pi D_p} \left(\frac{1-f_t}{\frac{\pi\rho_w}{8} D_p^2} \right)^{\frac{1}{2}} \right)^{-1}. \tag{76}$$

Focusing on the Diesel-generator sets, constraints on their power output are necessary to impose load sharing. For this reason, we need to define a matrix of dummy variables $\boldsymbol{d_{dg}} \in \mathbb{Z}_2^{k_{dg} \times k_{dg}}$ indicating if a pair of DGs are connected to the SB

$$\boldsymbol{d_{dg}} = 1 - \boldsymbol{z_{dg}} \boldsymbol{z_{dg}}^{\intercal}. \tag{77}$$

Therefore, load sharing can be imposed with the following constraints

$$-M \boldsymbol{d_{dg}} \leq \boldsymbol{u_{dg}} - \boldsymbol{u_{dg}}^{\intercal} \leq M \boldsymbol{d_{dg}}, \tag{78}$$

where M is a large enough constant.

Finally, an extra set of constraints is required, to force to zero the power output of DGs not connected to the SB

$$0 \leq \boldsymbol{u_{dg}} \leq \boldsymbol{z_{dg}} P_{dg,nom}, \tag{79}$$

where $P_{dg,nom}$ is the nominal power output of each DG.

B. Objective Functions

In this paper, we have considered three optimisation criteria:

(i) minimisation of the DGs fuel consumption with pitch control (our proposal);
(ii) minimisation of total propellers power
  (a) with pitch control;
  (b) without pitch control (proposed and discussed in [6], [34]–[37]);
(iii) minimisation of thrust delivered by the thrusters without pitch control (proposed in [1]).

Note that Problem (i) is our novel proposal, Problem (ii).(a) is an intermediate problem that we formulate for completeness, to assess the effect of considering the pitch as control variable in Problem (ii).(b), while Problems (ii).(b) and (iii) are state-of-the-art proposals available in literature.

For what concerns the fuel consumption minimisation problem (Problem (i)), the objective function can be formulated as the sum of the specific fuel consumption of the DGs, as reported in Eqns. (50)-(51)

$$\dot{m}_f = \sum_{i=1}^{k_{dg}} \left(u_{dg,i} z_{dg,i} \sum_{j=0}^{2} c_{dg,j} u_{dg,i}^{j} \right). \tag{80}$$

Regarding propeller power minimisation (Problem (ii)), we can derive the objective function, with (Problem (ii).(a)) or without (Problem (ii).(b)) pitch control, from Eqns. (22)-(28) it is possible to obtain

$$P_{tot,p} = \sigma_{12} \sum_{j=0}^{k_p} \left(\left(u_{x,j}^2 + u_{y,j}^2\right)^{\frac{3}{4}} \frac{\sum_{i=0}^{3} c_{q_0,i} \frac{u_{p,j}^i}{D_p^i}}{\left(\sum_{i=0}^{1} c_{t_0,i} \frac{u_{p,j}^i}{D_p^i}\right)^{\frac{3}{2}}} \right), \tag{81}$$

$$\sigma_{12} = \left(\frac{(1-f_t) T_{p,max}}{\pi \rho_w} \right)^{\frac{3}{2}} \frac{1}{\eta_r \pi^2 \left(0.7 D_p\right)^4}. \tag{82}$$

For Problem (ii).(b), we have assumed that all the elements of $\boldsymbol{u_p}$ are equal to the nominal pitch of the propeller (p_{nom})

$$P_{tot} = \sigma_{13} \sum_{j=0}^{k_p} \left(u_{x,j}^2 + u_{y,j}^2\right)^{\frac{3}{4}}, \tag{83}$$

$$\sigma_{13} = \frac{\left(8(1-f_t) T_{p,max}\right)^{\frac{3}{2}}}{\left(\pi \rho_w\right)^{\frac{3}{2}} \eta_r \pi^2 \left(0.7 D_p\right)^4} \frac{\sum_{i=0}^{3} \left(c_{q_0,i} \frac{p_{nom}^i}{D_p^i}\right)}{\left(\sum_{i=0}^{1} c_{t_0,i} \frac{p_{nom}^i}{D_p^i}\right)^{\frac{3}{2}}}. \tag{84}$$

Finally, for the minimisation of total thrust without pitch control (Problem (iii)), the objective function is the sum of all the elements of the vector $\boldsymbol{u_t}$

$$T_{tot} = \sum_{i=0}^{k_p} \left(u_{x,i}^2 + u_{y,i}^2\right)^{\frac{1}{2}}. \tag{85}$$

C. Simplifications of the Optimisation Problems

As a starting point, let us note that

- Problem (i) is a mixed-binary programming problem with non convex objective and non-linear constraints;
- Problem (ii). (a) is a continuous non-convex, non-linearly constrained optimisation problem;
- Problem (ii). (b) is a continuous convex, non-linearly constrained optimisation problem [1], [6];
- Problem (iii) is a continuous convex, non-linearly constrained optimisation problem [1], [6].

Note that for Problem (ii).(b) and Problem (iii) a number of solution methods have been proposed [80]–[82].

Problem (i) is obviously a very difficult combinatorial problem which may be hard to solve in a nearly-real time as required in real-life DP applications. For this reason, in order to meet these requirements, we have to apply a series of theoretically or physically grounded simplifications which, from one side, allow to find a minimum thrust in nearly-real time and, from the other side, still take into account all the physical phenomena (e.g. fuel consumption, pitch, and thrust direction and intensity) [83]–[92].

The first and trivial step, is to reduce the dimensionality of all problems, eliminating all the equality constraints of Eq. (57) by substituting them inside the objective functions and the inequality constraints [83], [88], [93], [94]. Hence, we expressed x- and y- thrust components of the first thruster (see in Figure 3 $u_{x,1}$ and $u_{y,1}$) and the x-component of the fourth thruster (see in Figure 3 $u_{x,4}$)

$$u_{x,1} = \frac{1}{\sigma_1} f_{env,u} - \sum_{i=2}^{k_p} u_{x,i}, \tag{86}$$

$$u_{y,1} = \frac{1}{\sigma_1} f_{env,v} - \sum_{i=2}^{k_p} u_{y,i}, \tag{87}$$

$$\frac{u_{x,4}}{h_{y,4}} = \frac{1}{\sigma_1} f_{env,y} + h_{x,4} u_{y,4} - \sum_{\substack{i=1 \\ i \neq 4}}^{k_p} h_{y,i} u_{x,i} - h_{x,i} u_{y,i}. \tag{88}$$

As a second step we eliminate the binary variable vector z_{dg}, the control vector $\boldsymbol{u_{dg}}$, and the load sharing constraints of Eqns. (78) and (79) in order to reduce the number of decision variables from twelve to two, without really changing the original problem, namely we simply reformulate the original optimisation problem with less variables. For this purpose, we have to introduce two new decision variables N_{dg} and u_{dg}. $N_{dg} \in \{1,2,3,4\}$ is the number of DGs connected to the SB, and u_{dg} is their, equal for all, power output. Then, we can reformulate the load balance across the main SB of Eq. (60) and the objective function of Eq. (51) as follows

$$N_{dg} u_{dg} = g, \tag{89}$$

$$\dot{m}_f = N_{dg} u_{dg} \sum_{j=0}^{2} c_{dg,j} u_{dg}^{j}. \tag{90}$$

$g = g(\boldsymbol{u_x}, \boldsymbol{u_y}, \boldsymbol{u_p})$ is the total power demand on the right hand side of Eq. (60).

Finally let us observe, also by means of Figure 8, that the specific fuel consumption behaviour provided by the manufacturer, suggests us that it is better to operate each DG

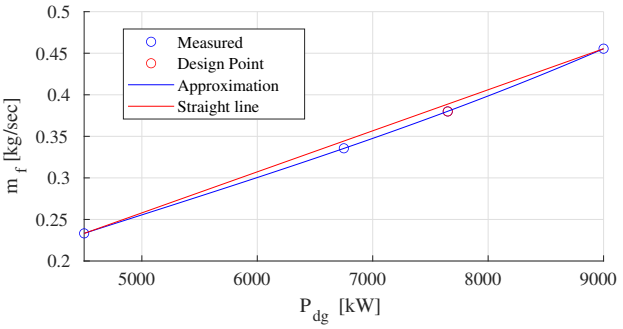

Figure 10: Fuel consumption as function of the delivered power of each DG.

Table IV: Optimisation problem summary

Problem	Number/Type of Variables	Objective. Eq.	Constraints Eqns.
(i)-Original	24 continuous 6 Binary	(80)	(55), (57), (60) (66), (68), (75), (78), (79)
(i)-Equivalent	18 continuous	(90)	(55), (66), (68), (75)
(ii).(a)	18 continuous	(81)	(55), (57), (66), (68), (75)
(ii).(b)	12 continuous	(83)	(55), (57), (66)
(iii)	12 continuous	(85)	(55), (57), (66)

close to its design point (red point in Figure 8). In other words, it is common practice to implement the on board PMSs in order to operate the vessels with all the DGs operating at their maximum efficiencies, and to turn on and off the number of DG according to this strategy. Nevertheless, let us plot in Figure 10 the total fuel consumption m_f, which is what we want to minimise as function of the delivered power

$$m_f = P_{dg} \cdot s_{fc} \tag{91}$$

for a particular DG, where P_{dg} and s_{fc} have been derived by means of the approximation of Figure 8. From Figure 10 it is possible to note that this function is very close to linearity. Consequently, Figure 10 tells us that, to deliver a particular power, we can both (i) turn on all the DGs and split equally the load, or (ii) turn on just the minimum number of DGs required to deliver the requested power. Both options (i) and (ii) would not change significantly the total fuel consumption. For this reason, exploiting the observation on specific fuel consumption, we chose the (ii) option since it guarantees to us that DG will work more close tho the design point. Based on this comments we can also eliminate N_{dg} and u_{dg} as we they can be directly derived from Eqns. (92)-(93) as follows

$$N_{dg} = \lceil \frac{g}{P_{dg,max}} \rceil, \tag{92}$$

$$u_{dg} = \frac{g}{N_{dg}}. \tag{93}$$

This practical and theoretically grounded approximation allows us to further simplify the problem and make it more manageable for near-real time optimisation.

For the convenience of the reader, we have summarised in Table IV the different optimisation problems reporting their objective functions and constraints.

D. Solution Methods

In order to solve the optimisation problems depicted in Section III, we employed different optimisation algorithms, namely Genetic Algorithm (GA), Particle Swarm Optimisation (PSO), and a Hybrid PSO with Interior Point method (PSO-IPM). In fact, other methods (e.g. gradient based or surrogates) were not able to handle the different optimisation problems which require the minimisation of highly non-linear objective functions subject to highly non-linear constraints. Moreover, practical applications, such as the thrust allocation problem for marine dynamic positioning systems, require the use of standard libraries and methods stable enough to be employed in daily practice. Hence, GA, PSO, and PSO-IPM are natural choices since they are standard, robust, and reliable methods available in most numerical platforms.

1) Genetic Algorithm (GA): GAs are a family of adaptive search procedures that have been described, extensively analysed, and successfully employed in the literature [95]–[102]. They derive their name from the fact that they are based on models of genetic change in a population of individuals. These models consist of three basic elements: (i) a Darwinian notion of "fitness", which governs the extent to which an individual can influence future generations, (ii) a "mating operator", which produces offsprings for the next generation, and (iii) genetic operators that determine the "genetic makeup" of the offsprings based on the genetic material of their parents [103]. There is a large body of both theoretical and empirical evidence showing that, even for very large and complex search spaces, GAs can rapidly locate regions with high fitness ratings [72].

For all the problems reported in Table IV, we employed 1000 individuals per generation, whose fitness scores were scaled according to their rank (r) as $1/\sqrt{r}$, in order to allow the evolution of more diverse populations. 5% of the fittest individuals were copied directly to the next generation, and for the remaining, stochastic uniform selection was employed. Finally, we exploited scattered crossover with probability of 80%, along with Gaussian mutation. For Problem (i)-Original, we exploited the MI-LXPM GA algorithm of [104]. In brief, it consists of extended Laplace crossover and Power mutation operators, along with a truncation procedure for the integer restrictions. The constraint handling method of [105] is employed, along with the tournament selection operator. In this case, the number of individuals in each population was increased to 1800, with a crossover probability rate of 90%, an Elite count of 10% of the population, and binary tournament selection. For Problems (ii).(a) and (iii), the Augmented Lagrangian Genetic Algorithm (ALGA) was employed [106], with the constraint handling method proposed in [105].

2) Particle Swarm Optimisation (PSO): PSO was originally developed by [107], [108]. The method was inspired by the behaviour of social organisms in groups, such as bird and fish schooling or ant colonies, and emulates the interaction between members to share information. The search of the optimal solution is performed through agents, referred to as particles, whose trajectories are adjusted by a stochastic and a deterministic component. Each particle has a position and a velocity in the search space, and, at every iteration, each particle trends towards the optimum based on its "best" achieved position and the group's "best" position. The movement of the

particles in the swarm is controlled by the cognitive and the social parameters, indicating the confidence of the particle in itself and in the swarm, respectively, and the inertial weight which influences the convergence behaviour by increasing the distance the particle will travel from its previous position. At the beginning of the optimisation, the PSO algorithm generates a random population of particles over the search space, where the position of each particle represents a solution. These particles are evaluated by computing the values of the objective function to obtain a fitness score, based on which the new position of each particle can be evaluated. The advantages of PSO is the reduced number of parameters to tune, constraints acceptance and speed in providing good solutions [109], [110]. Furthermore, the stochastic properties of the algorithm allow for solution variability and thorough exploration of the search space in the initial iterations, with a local search behaviour during the final iterations [111].

For all the problems reported in Table IV excluding Problem (i)-Original (which cannot be addressed with PSO since it does not handle properly discrete variables), we set the swarm size to 180 particles, and the initial particles were randomly and uniformly distributed on the search space. We applied linearly decreasing inertia with a starting value of 1.1, and set the velocity of each particle to be influenced by a local neighbourhood of 90% of the entire swarm. Finally, for the velocity adjustment of each particle between iterations, the relative weighting of each particle's best position and the local neighbourhood's best position were both set to 1.49.

However, when applied in highly non-linear problems, PSO is known to converge to sub-optimal solutions, and its behaviour is rather sensitive with respect to its parameters [112]–[114]. Although several studies have been dedicated to its convergence analysis [115]–[119], how to properly adjust its control parameters to achieve good performance is still an open issue.

3) Hybrid PSO with Interior Point method (IPM): To mitigate the PSO problems, we decided to test the the PSO-IPM algorithms, in which the best value of all particles in PSO, being close to an optimum point, is given as the initial starting point for the IPM, to perform a more efficient local search. IPMs originate from [120], whereas the modern era of IPM started with the work of [121]. They are classified into three main categories: projective methods, affine-scaling methods, and primal-dual methods. Among the different IPMs, the primal-dual algorithms have gained a reputation for being the most efficient, which is the reason why we employ them here. In brief, optimality with every IPM is achieved through the following steps: transforming an inequality constrained optimisation problem to equality constrained one, formulate the Lagrange function using logarithmic barrier functions, set the first-order optimality conditions, and apply Newton's method to the set of equations coming from these optimality conditions.

For PSO-IPM, the parameters have been set as in the PSO algorithm.

IV. Results

In this section we will analyse the results of exploiting the different optimisation problems, summarised in Table IV, for DP operations with the optimisation algorithms described in Section III-D.

Table V: GA, PSO, and PSO-IPM parameters and addressed optimisation problem (see Table IV).

Algorithm	Parameter	Value/Type	Problem (Table IV)
GA (ALGA)	Initial Population	Uniform Sampling	(i)-Equivalent (ii).(a) (ii).(b) (iii)
	Population size	1000	
	Fitness scaling	Rank	
	Elitism	5%	
	Crossover type	Scattered	
	Crossover rate	80%	
	Selection function	Stochastic Uniform	
	Mutation type	Gaussian	
MI-LXPM GA	Initial Population	Uniform Sampling	(i)-Original
	Population size	1800	
	Fitness scaling	Rank	
	Elitism	10%	
	Crossover type	Extended Laplace	
	Crossover rate	90%	
	Selection function	Binary Tournament	
	Mutation type	Power	
PSO PSO-IPM	Initial swarm	Uniform Sampling	(i)-Equivalent (ii).(a) (ii).(b) (iii)
	Swarm size	180	
	Inertia weights	1.1, Linear Decrease	
	Neighbour fraction	90%	
	Self adjustment weight	1.49	
	Social adjustment weight	1.49	

In particular, we will first perform a number of checks on the physical plausibility of the the thrust allocation found by the optimisation algorithm. Then we will study the fuel consumption savings when the proposed modelisations are exploited instead of the state-of-the-art ones.

All experiments were performed on a machine equipped with two Intel Xeon Silver 4216, 128 GB of RAM, and 512 GB SSD running Windows Server 2019 and equipped with Matlab R2020a. Matlab R2020a already implements the GA in the function *ga*, the PSO in the function *pso*, and the IPM algorithm in the function *fmincon*. The PSO-IPM hybrid approach can be easily performed by setting the *HybridFcn* option of *pso* to *fmincon*.

The parameters employed for the GA, the PSO, and the PSO-IPM optimisation algorithms are summarised in Table V. This parameters have been chosen to obtain the best results (minimum cost) through all the experiments. In Table V are also reported the optimisation problems of Table IV solved with the specific optimisation algorithm.

Before presenting our results, we want to make clear that even with extensive parameter tuning, the MI-LXPM GA could not solve the majority of the instances of Problem (i)-Original even with many hours of computation. This made clear the necessity of switching from Problem (i)-Original to Problem (i)-Equivalent as described in Section III-C. For this reason, from now on, we will report only the results of Problems (i)-Equivalent, (ii).(a), (ii).(b), and (iii).

The rest of this section is organised as follows. Section IV-A reports the analysis, from a physical point of view, of the solutions of Problem (i)-Equivalent in a particular environmental condition. Then Section IV-B illustrates the performance of the different DP problems of Table IV, using also the different optimisers (see Section III-D), in terms of fuel consumption, fuel savings, and computational requirements.

A. Physical Plausibility

To ensure the alignment between the results of the thrust allocation and the DP physical problem, we carried out a number of physical plausibility checks. In particular, we chose Problem (i)-Equivalent for these check since, compared with the other problems, it is the most exhaustive and physically accurate model (see Section III). Moreover, it guarantees the minimum fuel consumption (see Sections IV-B) and it is effectively exploitable in operations with standard optimisation algorithms in near real time (see Section IV-B4).

Figures 11(a)-11(e) report the solutions to Problem (i)-Equivalent for 5 different operating conditions, in terms of relative wind speed V_{rw} and direction γ_{rw} of the environmental forces. In particular, for $\gamma_{rw} = \{0^o, 45^o, 90^o, 135^o, 180^o\}$, namely Figures 11(a)-11(e), we considered V_{rw} as the maximum value that the vessel can sustain while still being able to maintain its position. This operating point is referred to, in literature, as maximum capability [1]. Note that $\gamma_{rw} = \{-45^o, -90^o, -135^o\}$ are not reported since symmetric w.r.t. $\gamma_{rw} = \{45^o, 90^o, 135^o\}$. In each figure, we reported

- top left: the operating points of the DG sets (see also Section II-H and Figure 8);
- middle left: the operating points of the propellers (see also Section II-D and Figure 5);
- bottom left: the operating points of the electric motors (see also Section II-F and Figure 7);
- right: the delivered thrust configuration, namely a blue vector representing the thrust's direction and intensity of each thruster, and the direction and intensity of the environmental forces as red vector applied to the centre of gravity of the vessel.

We chose these specific conditions as they can be easily checked for their physical plausibility. In fact, since in Figures 11(a)-11(e) we are considering the maximum V_{rw} that the vessel can sustain, still being able to maintain its position, it is reasonable to assume that the DGs, the thrusters, and the EMs will work in similar operating condition, in terms of delivered total thrust and requested total power. In order to support this statement, in Table VI we reported, for each considered conditions of Figures 11(a)-11(e), the total trust, the total EMs power, and total DGs power. As expected, all the reported condition are sharing a similar lever of total trust, total EMs power, and total DGs power.

From the results reported in Figures 11(a)-11(e) we can make a series of observations

- as expected the selected wind direction and speed puts the system in a state for which it should operate near their design point. In fact, the vessel exploits all the 5 DGs operating approximately at 74% of their maximum power to sustain the maxim wind speed at different angles. It is easy to verify that the operation of 4 or 6 DG sets for the same load would result in higher fuel consumption;
- as expected (see Section II-D), all the propellers operate at their design pitch, maximising their efficiency;
- as expected (see Section II-F), the induction motors operate at at their most efficient region, with an efficiency of 0.96, very close to their nominal point;
- in Figures 11(a) and 11(e) we can note that the thrusters produce thrust in exactly the opposite direction from the environmental forces. This is possible, because for these operating conditions there is no interaction between any two thrusters. Note that, considering Eqns. (90) and (60), any other thrust configurations with non-zero forces on the lateral ship axis $u_{y,i}$ would result in the production of unnecessary additional power from the DG sets, which subsequently would increase total fuel consumption;
- in Figure 11(c), the environmental conditions act only on the lateral axis of the vessel. Figure 11(c) shows that the forbidden zone constraints (see Section III-A) prevent the thrusters from operating solely on the lateral direction due to thruster-thruster flow interaction. We can verify, with the support of Table VI, that this is the optimal thrust configuration as it requires the same amount of total DGs power of the conditions reported in Figures 11(a) and 11(e). Instead, the EMs operate at slightly different points of lower rotational speed and higher torque, however their efficiency is still equal to the highest possible value of 0.96. Finally, we can see that the thrust configuration of the two thruster triplets on the fore and aft of the vessel is not symmetrical. This is due to the asymmetry of the hull on the fore and aft of the vessel which produces a certain moment on the yaw direction that has to be accounted for, in order to keep the vessel in a stationary position on the earth-fixed reference frame.
- we can also verify that the solutions of reported in Figures 11(b) and 11(d) are physically reasonable, although the optimal solution is far from trivial to identify, primarily due to the forbidden zone constraints. Once again, all components are operating near their nominal point, with the exception of the induction motors, which still operate at their most efficient region. The same amount of power is produced by the DG sets, with 5 of them operating near the most efficient operating point to satisfy power demand, while still satisfying the load sharing constraints.

B. Performance

In this section we will first compare the performance, in terms of fuel consumption and savings, of the different problems reported in DP optimisation problem summarised in Table IV in different conditions

- All Conditions (Section IV-B2): in this case we fix the sea state (to the average behaviour in a specific geographical position) and we vary the wind intensity and direction;
- In Operation (Section IV-B3): in this case we simulate the use of the DP algorithms in real operations for North Atlantic and North Pacific sea regions.

By means of this results we will be able to show that Problem (i)-Equivalent is actually the best performing one in terms of fuel consumption and savings.

Then, in Section IV-B4 we study the trade-off between the computational requirements and the optimality of the solution taking into account different optimisation algorithms (see Section III-D) for solving Problem (i)-Equivalent.

In order to present all these results, it is necessary to introduce the concept of Capability Plot (CP), that will be instrumental to present the results in an intelligible way.

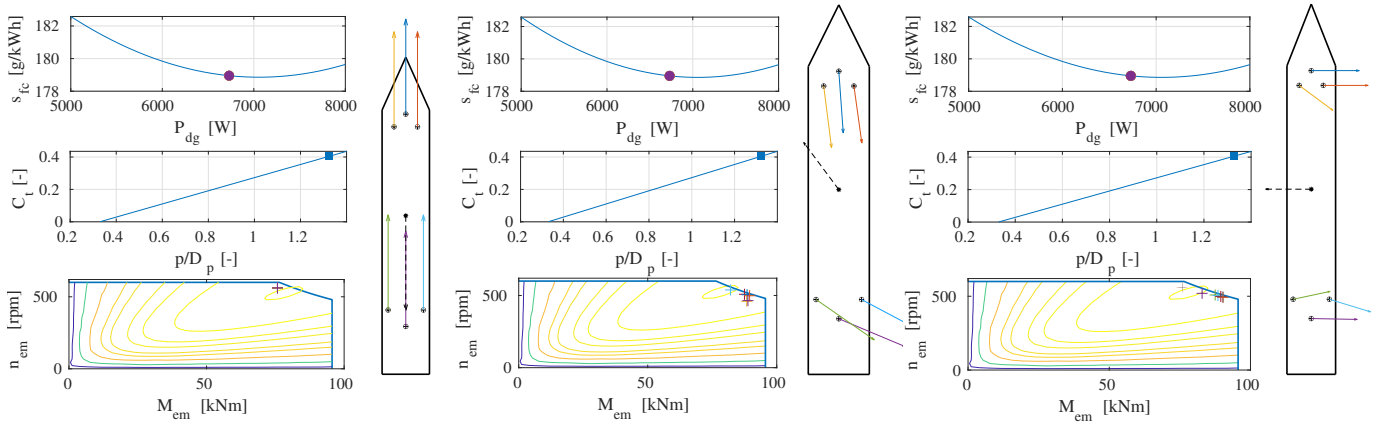

(a) $V_{rw} = 100\ m/s, \gamma_{rw} = 0^{o}$ (b) $V_{rw} = 27\ m/s, \gamma_{rw} = 45^{o}$ (c) $V_{rw} = 37\ m/s, \gamma_{rw} = 90^{o}$

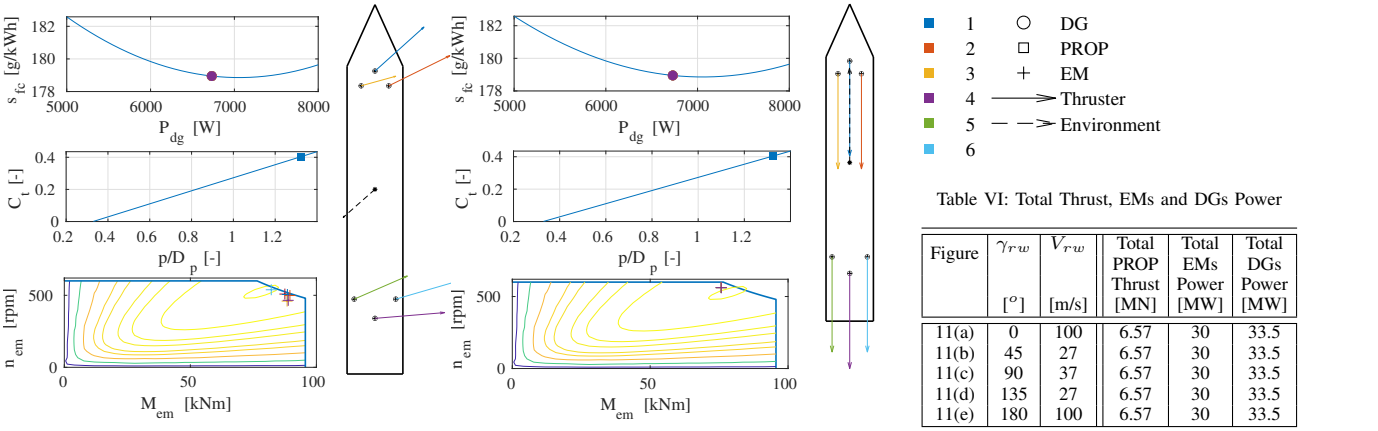

(d) $V_{rw} = 27\ m/s, \gamma_{rw} = 135^{o}$ (e) $V_{rw} = 100\ m/s, \gamma_{rw} = 180^{o}$

Figure 11: Physical Check

Table VI: Total Thrust, EMs and DGs Power

Figure	γ_{rw} [^{o}]	V_{rw} [m/s]	Total PROP Thrust [MN]	Total EMs Power [MW]	Total DGs Power [MW]
11(a)	0	100	6.57	30	33.5
11(b)	45	27	6.57	30	33.5
11(c)	90	37	6.57	30	33.5
11(d)	135	27	6.57	30	33.5
11(e)	180	100	6.57	30	33.5

1) Capability Plot: The DP CP is a crucial tool to assess a vessel's ability to retain its heading and position under certain environmental conditions [1]. Based on a given vessel design, the capability plots consider the total environmental forces (due to wind, waves, and ocean currents) both in terms of direction and intensity.

In particular, to build the capability plot, it is necessary

- to vary the wind direction $\gamma_{rw} \in \{0, \cdots, 360\}$ and speed V_{rw}. The rage of the speed will be clarified soon;
- to fix the waves and the ocean currents intensity to their (e.g. considering the average significant wave high in Section II-C Eqns. 10 and 11) while vary their direction in accordance with the wind direction. Namely one has to consider the worst case scenario in which the wind, waves, and currents are acting in the same direction;
- to compute the trust allocation in accordance with the formulations reported in Table IV;
- to increase $V_{rw} \in [0, ...)$ until the vessel is able to maintain its stationary position, namely the environmental forces are balanced by the thrust offered by the thruster configuration;
- to report, for each γ_{rw} and V_{rw}, the desired quantity[1] (e.g. fuel consumption or fuel savings). The latter is presented on a polar plot where γ_{rw} is the angle coordinate and V_{rw} is the distance coordinate.

We assume that 0^o corresponds to forces acting on the bow, and 180^o corresponds to forces acting on the stern of the vessel.

2) Fuel Savings - All Conditions: In Figure 12 we report different CPs when the sea state has been fixed to moderate (degree 4 in the Douglas sea scale according to the World Meteorological Organization) since it is the most frequent sea state according to [122].

Figures 12(a)-12(d) report the fuel consumption of each DP optimisation problem of Table IV, apart from Problem (i)-Original. In fact, even with extensive parameter tuning, the MI-LXPM GA failed to solve the majority of the instances of Problem (i)-Original, even at run-times an order of magnitude higher than the ALGA in Problem (i)-Equivalent. As we can see from Figures 12(a)-12(d), the fuel consumption seems to be similar regardless of the DP optimisation problem exploited.

[1]Note that, the conventional capability plot just reports the maximum V_{rw} [1]

Table VII: Sea states, probability of occurrence in North Atlantic and North Pacific, and related fuel savings using Problems (i), (ii).(a), and (ii).(b) with respect to Problem (iii).

Sea State	$Vw\ [m/s]$ min	max	mean	Probability occurrence [%] North Atlantic	North Pacific	Average fuel savings w.r.t to Problem (iii) Problem (i)	Problem (ii).(a)	Problem (ii).(b)
1	0.00	2.81	1.40	0	0	4.480	2.967	0.002
2	3.27	4.68	3.97	7.2	4.1	4.414	2.900	0.001
3	5.14	7.48	6.31	22.4	16.9	4.298	2.840	0.001
4	7.95	9.82	8.88	28.7	27.8	4.180	2.760	0.002
5	10.29	12.62	11.46	15.5	23.5	4.050	2.680	0.001
6	13.09	21.98	17.53	18.7	16.3	3.700	2.450	0.001
7	22.44	25.72	24.08	6.1	9.1	3.204	2.116	0.000
8	26.19	29.46	27.82	1.2	2.2	2.872	1.917	0.000
>8	>29.46			0.05	0.1	0.598	0.399	0.000

However, by examining the relative fuel savings achieved by Problems (i), (ii).(a), and (ii).(b) against Problem (iii), as reported in Figures 12(e)-12(g), the advantage of using more complex and detailed DP optimisation problem becomes evident. From Figure 12(e) it is possible to observe that if instead of minimising for total thrust according to Problem (iii), one minimises the fuel consumption according to Problem (i)-Equivalent results in fuel savings up to 6% for very low wind speeds and very low environmental forces. Problem (ii).(a) results in lowers saving (up to 4%). Finally, Problem (ii).(b) provides essentially no additional savings. This result is expected, as the objective functions of Problem (ii).(b) and Problem (iii) are equivalent, and just the constraints change (see Table IV).

Finally, in order to better appreciate the fuel savings of Problems (i), (ii).(a), and (ii).(b) with respect to Problem (iii), in Figure 12(h) we report the fuel savings in the CP distribution and their averaged values. Clearly Problem (i)-Equivalent guarantees the best saving and Problems (i)-Equivalent, (ii).(a), (ii).(b) provide an average fuel saving of 3.12%, 2.06% and 0.01%, respectively.

3) Fuel Savings - In Operations: To assess the benefits of using the newly proposed DP optimisation problems in actual operating conditions we exploited the wind and wave (the sea state according to the Douglas sea scale) data of the North Atlantic and North Pacific area that were collected during an extensive measurement campaign in [122] together with their probability of occurrence. These data are reported in Table VII. In the same table it is also reported the average fuel savings, in that particular sea state, when using Problems (i), (ii).(a), and (ii).(b) against Problem (iii). Note that, as expected and also commented in Section IV-B2, Problem (i) guaranties the largest savings in all sea states and the largest savings are achieved in lower sea states.

Since the probability of occurrences of each sea state in the North Atlantic and North Pacific area we can also estimate the lifetime average fuel savings using Problems (i), (ii).(a), and (ii).(b) with respect to Problem (iii). These quantities are reported in Table VIII. From this table it is possible to observe that, using Problem (i), guaranties and approximately extra 4% fuel savings in both regions.

4) Computational Requirements: In Figure 13 we report different CPs in the same conditions described in Section IV-B2 for Figure 12.

In particular Figures 13(a)-13(c) report the fuel consumption for Problem (i)-Equivalent (the best performing one according to the results of Sections IV-B2 and IV-B3) using the different optimisers (GA, PSO-IPM, and PSO) described in Section III-D. By observing Figures 13(a)-13(b), the fuel consumption seems to be similar regardless of the exploited optimiser (GA or PSO-IPM) while for PSO the behaviour is quite different. In order to better understand these results, in Figures 13(d)-13(e) we reported the percentage of fuel savings using, respectively the PSO-IPM and PSO optimisers against the GA optimiser. From these results it is possible to observe that the PSO-IPM optimiser is slightly worse than the GA while the PSO is largely worse than GA.

Table VIII: Lifetime average fuel savings in North Atlantic and North Pacific using Problems (i), (ii).(a), and (ii).(b) with respect to Problem (iii).

Problem	Lifetime Average Fuel Savings [%]	
	North Atlantic	North Pacific
Problem (i)	4.04	3.98
Problem (a)	2.67	2.63
Problem (b)	0.001	0.001

Moreover, Figures 13(f)-13(h) report the time required to find the optimal solution, still for Problem (i)-Equivalent using the different optimisers. From Figures 13(a)-13(b) it is possible to note that the time seems to be very high for GA and very low for PSO, and, as intuitively expected, the time grows as we get close to the CPs limits. Also in this case, to provide the reader with a better understanding of the reported results, in Figures 13(i)-13(j) we reported the percentage of time savings using, respectively the PSO-IPM and PSO optimisers against the GA optimiser. From this results it is possible to observe that the PSO optimiser is the fastest method while the GA is the slowest. PSO-IPM is slightly slower than PSO.

From these results, it is possible to conclude that PSO-IPM is the method with the best trade-off between accuracy and computational requirement which allows to used Problem (i)-Equivalent in near real-time DP applications.

V. Conclusions

Marine DP systems play a central role in offshore maritime operations assuring the mission of the vessels (e.g. drill ling, pipe-laying, coring, and ocean observation) by maintaining the vessel's position and heading using its own propellers and thrusters to compensate exogenous disturbances, like wind, waves and currents. For these type of vessels, the DP system is the primary cause of fuel consumption having a strong impact on its overall footprint. For this reason this paper faced the problem of optimising the propellers thrust allocation, namely determining thrust and direction of each propeller and thruster, to maintain its position and heading, while minimising the fuel consumption.

State of the art approaches commonly exploit a simplified approach where simpler (mostly convex), yet related, optimisation problems are exploited as surrogates to keep the problem and the computational requirements at a level suited for a near-real time control. This allows to design a DP system able to operate in near-real time allowing its exploitation on-board during operation by simply integrating it in the automation system.

The novelty of the paper lies in the following aspects. Firstly, we propose to directly face the problem with a high

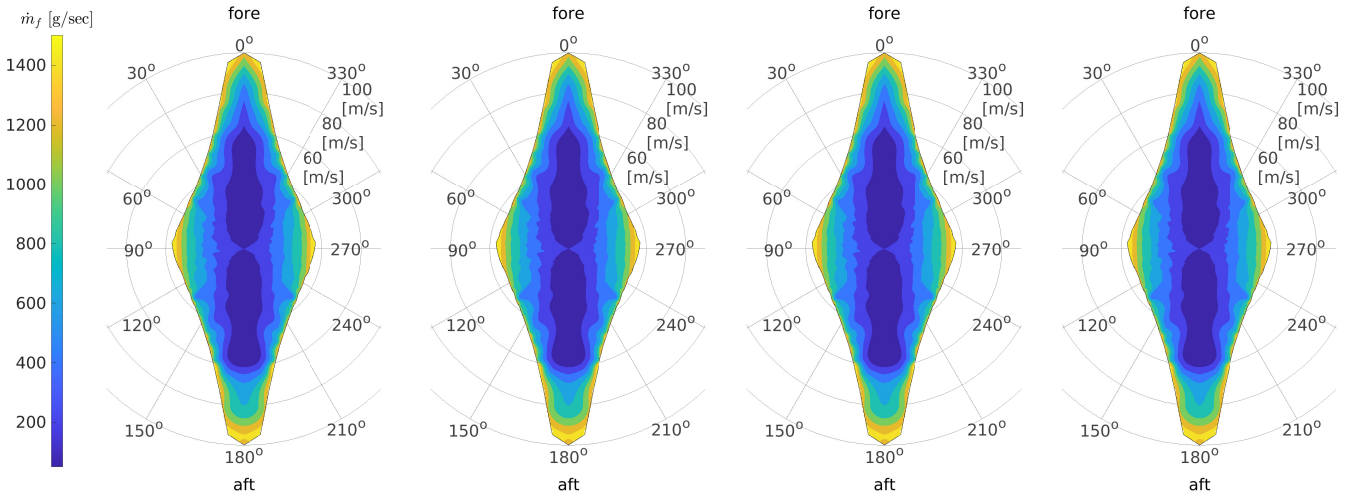

(a) Fuel consumption with Problem (i)

(b) Fuel consumption with Problem (ii).(a)

(c) Fuel consumption with Problem (ii).(b)

(d) Fuel consumption with Problem (iii)

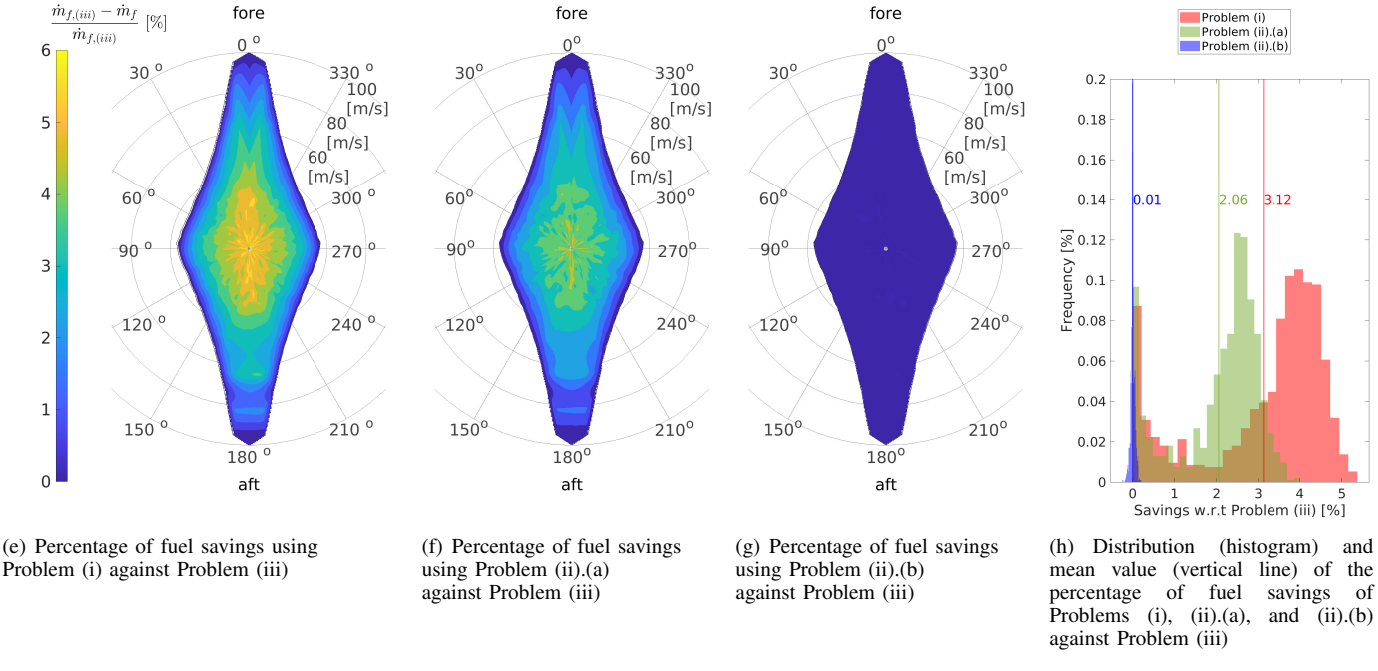

(e) Percentage of fuel savings using Problem (i) against Problem (iii)

(f) Percentage of fuel savings using Problem (ii).(a) against Problem (iii)

(g) Percentage of fuel savings using Problem (ii).(b) against Problem (iii)

(h) Distribution (histogram) and mean value (vertical line) of the percentage of fuel savings of Problems (i), (ii).(a), and (ii).(b) against Problem (iii)

Figure 12: DP Capability Plot with fuel consumption (top), and fuel savings with respect to Problem.(iii) (bottom)

fidelity modelling approach, secondly we exploit physical and theoretical funded proprietaries for the purpose of achieving optimal solutions in near-real time with standard optimisers.

Authors showcased the proposed approach applying their methodology on a drilling unit, equipped with six thrusters to evaluate the potential fuel consumption savings. Results showed show that it is possible to achieve up to 5% of fuel savings with respect to conventional approaches.

Nevertheless, space for improvement still exists. For example we could incorporate the thruster-thruster hydrodynamic interaction effects. In this work, the standard approach of avoiding these effects has been employed, by adding the forbidden zone constraints for some azimuth angles in which severe interaction occurs. However, authors of [3] indicate that additional benefits arise by representing these effects with thrust efficiency curves, instead of using forbidden zone constraints. Another improvement could related to the modelisation of frequent DG starts and stops. Although these effects have not been investigated in this work, it is known that frequently starts and stops are harmful for the lifetime of any internal combustion engine [123]. Another interesting direction of research could be to examine the performance of our approach aiming at directly reducing the emissions [123]. Finally, custom optimisers for the proposed DP problems could be developed targeting higher efficiency and effectiveness with respect to standard general purpose optimisers.

REFERENCES

[1] T. I. Fossen. *Handbook of marine craft hydrodynamics and motion control*. John Wiley & Sons, 2011.

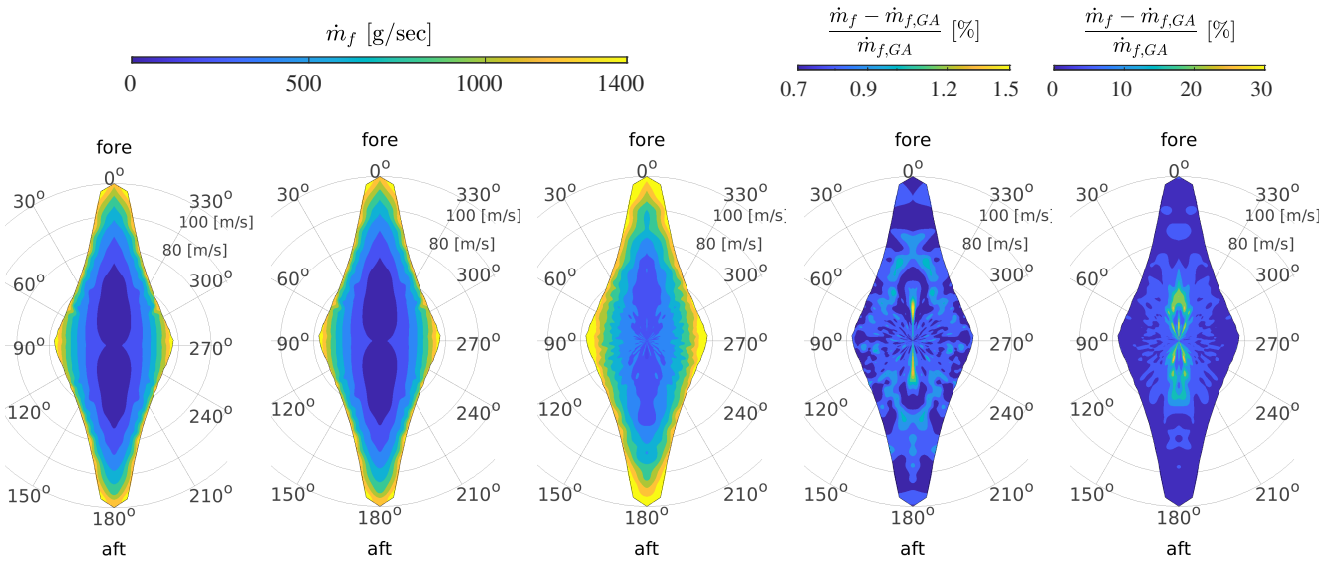

(a) Fuel consumption using the GA optimiser. (b) Fuel consumption using the PSO-IPM optimiser. (c) Fuel consumption using the PSO optimiser. (d) Percentage of fuel savings using PSO-IPM against GA (e) Percentage of fuel savings using PSO against GA

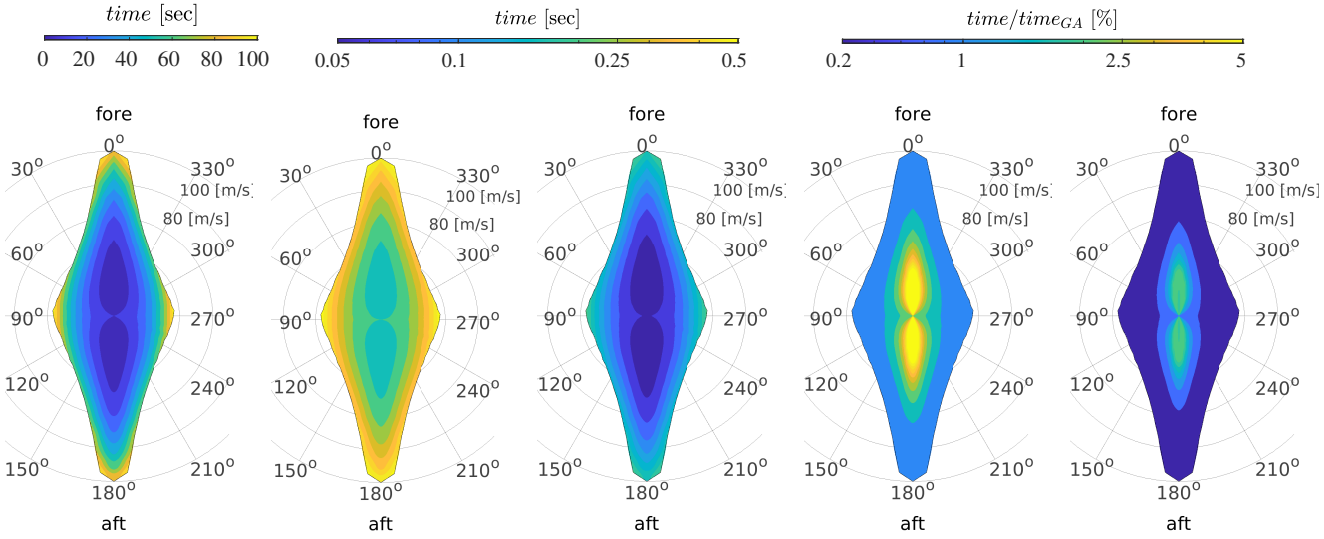

(f) Time using the GA optimiser. (g) Time using the PSO-IPM optimiser. (h) Time using the PSO optimiser. (i) Percentage of time savings using PSO-IPM against GA (j) Percentage of time savings using PSO against GA

Figure 13: DP Capability Plot with fuel consumption (top) and computational requirements (bottom) for the DP Problem (i)-Equivalent (the best performing one according to the results of Sections IV-B2 and IV-B3) using the different optimisers (GA, PSO-IPM, and PSO) described in Section III-D.

[2] T. I. Fossen. A survey on nonlinear ship control: from theory to practice. In *5th IFAC Conference on Manoeuvring and Control of Marine Craft*, 2000.

[3] F. Arditti, L. F. Souza, T. C. Martins, and E. A. Tannuri. Thrust allocation algorithm with efficiency function dependent on the azimuth angle of the actuators. *Ocean Engineering*, 105:206–216, 2015.

[4] E. A. Tannuri, D. C. Donha, and C. P. Pesce. Dynamic positioning of a turret moored fpso using sliding mode control. *International Journal of Robust and Nonlinear Control*, 11(13):1239–1256, 2001.

[5] A. Arapogianni, A. B. Genachte, and J. Moccia. The offshore wind market deployment: forecasts for 2020, 2030 and impacts on the european supply chain development. *Energy Procedia*, 24:2–10, 2012.

[6] E. Ruth. *Propulsion control and thrust allocation on marine vessels*. PhD thesis, Norwegian University of Science and Technology, 7 2008.

[7] J. G. Balchen, N. A. Jenssen, and S. Sælid. Dynamic positioning using kalman filtering and optimal control theory. In *IFAC/IFIP symposium on automation in offshore oil field operation*, 1976.

[8] S. Saelid, N. Jenssen, and J. Balchen. Design and analysis of a dynamic positioning system based on kalman filtering and optimal control. *IEEE Transactions on Automatic Control*, 28(3):331–339, 1983.

[9] M. J. Grimble and M. A. Johnson. *Optimal control and stochastic estimation: theory and applications*. John Wiley & Sons, Inc., 1986.

[10] T. I. Fossen, S. I. Sagatun, and A. J. Sørensen. Identification of dynamically positioned ships. *Control Engineering Practice*, 4(3):369–376, 1996.

[11] E. A. Tannuri and D. C. Donha. H∞ controller design for dynamic positioning of a turret moored fpso. In *5th IFAC Conference on Manoeuvring and Control of Marine Craft*, 2000.

[12] T. Perez and A. Donaire. Constrained control design for dynamic positioning of marine vehicles with control allocation. *Modelling, Identification and Control*, 30(2):57–70, 2009.

[13] I. Popov, P. Koschorrek, A. Haghani, and T. Jeinsch. Adaptive kalman filtering for dynamic positioning of marine vessels. In *20th IFAC World Congress*, 2017.

[14] W. Shibo, Z. Boyuan, W. Shijia, and G. Shirong. Dynamic precise positioning method of shearer based on closing path optimal estimation model. *IEEE Transactions on Automation Science and Engineering*, 16(3):1468–1475, 2018.

[15] A. Jayasiri, A. Nandan, S. Imtiaz, D. Spencer, S. Islam, and S. Ahmed. Dynamic positioning of vessels using a ukf-based observer and an nmpc-based controller. *IEEE Transactions on Automation Science and Engineering*, 14(4):1778–1785, 2017.

[16] R. I. Stephens, K. J. Burnham, and P. J. Reeve. A practical approach to the design of fuzzy controllers with application to dynamic ship positioning. In *3rd IFAC Workshop on Control Applications in Marine Systems*, 1995.

[17] T. I. Fossen and A. Grovlen. Nonlinear output feedback control of dynamically positioned ships using vectorial observer backstepping. *IEEE transactions on control systems technology*, 6(1):121–128, 1998.

[18] E. A. Tannuri, A. C. Agostinho, H. M. Morishita, and L. Moratelli Jr. Dynamic positioning systems: An experimental analysis of sliding mode control. *Control engineering practice*, 18(10):1121–1132, 2010.

[19] S. K. Volovodov, A. V. Smolnikov, S. S. Volovodov, and B. P. Lampe. Synthesis of exponentially stable dynamic positioning systems for sea mobile objects using lyapunov's method. In *Maritime Electronic Symposium*, pages 4271–4276, 2007.

[20] P. Sinding and S. V. Andersen. A force allocation strategy for dynamic positioning. In *The 8th International Offshore and Polar Engineering Conference*, 1998.

[21] J. P. Hespanha and A. S. Morse. Switching between stabilizing controllers. *Automatica*, 38(11):1905–1917, 2002.

[22] J. P. Hespanha, D. Liberzon, and A. S. Morse. Hysteresis-based switching algorithms for supervisory control of uncertain systems. *Automatica*, 39(2):263–272, 2003.

[23] A. J. Sørensen, S. T. Quek, and T. D. Nguyen. Improved operability and safety of dp vessels using hybrid control concept. In *International Conference on Technology & Operation of Offshore Support Vessels*, 2005.

[24] T. D. Nguyen, A. J. Sørensen, and S. T. Quek. Design of hybrid controller for dynamic positioning from calm to extreme sea conditions. *Automatica*, 43(5):768–785, 2007.

[25] M. Blanke, M. Kinnaert, J. Lunze, M. Staroswiecki, and J. Schröder. *Diagnosis and fault-tolerant control*. Springer, 2006.

[26] D. T. Nguyen, M. Blanke, and A. J. Sørensen. Diagnosis and fault-tolerant control for thruster-assisted position mooring. In *7th IFAC Conference on Control Applications in Marine Systems*, 2007.

[27] S. Fang and M. Blanke. Fault monitoring and fault recovery control for position-moored vessels. *International Journal of Applied Mathematics and Computer Science*, 21(3):467–478, 2011.

[28] H. Faÿ. *Dynamic Positioning Systems: Principles, Design, and Applications*. Ophrys Editions, 1990.

[29] T. I. Fossen and T. A. Johansen. A survey of control allocation methods for ships and underwater vehicles. In *14th Mediterranean Conference on Control and Automation*, pages 1–6, 2006.

[30] A. J. Sørensen. A survey of dynamic positioning control systems. *Annual reviews in control*, 35(1):123–136, 2011.

[31] M. Bodson. Evaluation of optimization methods for control allocation. *Journal of Guidance, Control, and Dynamics*, 25(4):703–711, 2002.

[32] S. M. Hasan. *A Procedure for the Dynamic Positioning Estimation in Initial Ship-Design*. PhD thesis, Université de Liège, 2018.

[33] A. Veksler, T. A. Johansen, and R. Skjetne. Transient power control in dynamic positioning-governor feedforward and dynamic thrust allocation. In *9th IFAC Conference on Manoeuvring and Control of Marine Craft*, 2011.

[34] D. Wu, F. Ren, and W. Zhang. An energy optimal thrust allocation method for the marine dynamic positioning system based on adaptive hybrid artificial bee colony algorithm. *Ocean Engineering*, 118:216–226, 2016.

[35] A. Baldini, A. Fasano, R. Felicetti, A. Freddi, S. Longhi, and A. Monteriù. A constrained thrust allocation algorithm for remotely operated vehicles. In *11th IFAC Conference on Control Applications in Marine Systems, Robotics, and Vehicles*, 2018.

[36] N. A. Jenssen and B. Realfsen. Power optimal thruster allocation. In *Dynamic positioning conference*, 2006.

[37] A. Veksler, T. A. Johansen, and R. Skjetne. Thrust allocation with power management functionality on dynamically positioned vessels. In *2012 American Control Conference*, 2012.

[38] E. Ruth, O. N. Smogeli, T. Perez, and A. J. Sorensen. Antispin thrust allocation for marine vessels. *IEEE Transactions on Control Systems Technology*, 17(6):1257–1269, 2009.

[39] M. Rindaroey and T. A. Johansen. Fuel optimal thrust allocation in dynamic positioning. In *9th IFAC Conference on Control Applications in Marine Systems*, 2013.

[40] S. Kim and M. Kim. Fuel-optimal thrust-allocation algorithm using penalty optimization programming for dynamic-positioning-controlled offshore platforms. *Energies*, 11(8):2128–2152, 2018.

[41] K. P. Lindegaard and T. I. Fossen. Fuel-efficient rudder and propeller control allocation for marine craft: Experiments with a model ship. *IEEE Transactions on Control Systems Technology*, 11(6):850–862, 2003.

[42] T. A. Johansen, T. I. Fossen, and P. Tøndel. Efficient optimal constrained control allocation via multiparametric programming. *Journal of guidance, control, and dynamics*, 28(3):506–515, 2005.

[43] C. C. Liang and W. H. Cheng. The optimum control of thruster system for dynamically positioned vessels. *Ocean Engineering*, 31:97–110, 2004.

[44] T. A. Johansen, T. P. Fuglseth, P. Tøndel, and T. I. Fossen. Optimal constrained control allocation in marine surface vessels with rudders. *Control Engineering Practice*, 16(4):457–464, 2008.

[45] E. Ruth and A. J. Sørensen. A solution to the nonconvex linearly constrained quadrating thrust allocation problem. In *8th IFAC Conference on Manoeuvring and Control of Marine Craft*, 2009.

[46] J. F. Hansen. *Modelling and control of marine power systems*. PhD thesis, Norwegian University of Science and Technology, 7 2000.

[47] D. Radan. *Integrated control of marine electrical power systems*. PhD thesis, Norwegian University of Science and Technology, 7 2009.

[48] F. Arditti and E. A. Tannuri. Experimental analysis of a thrust allocation algorithm for dp systems considering the interference between thrusters and thruster-hull. In *9th IFAC Conference on Manoeuvring and Control of Marine Craft*, 2012.

[49] F. Ren, D. Wu, G. Yang, and Z. Yin. An intelligent thrust allocation method for dynamic positioning based on enhanced artificial bee colony algorithm. In *9th IEEE Conference on Industrial Electronics and Applications*, 2014.

[50] E. F. G. Van Daalen, J. L. Cozijn, C. Loussouarn, and P. W. Hemker. A generic optimization algorithm for the allocation of dp actuators. In *30th International Conference on Ocean, Offshore and Arctic Engineering*, 2011.

[51] F. Arditti, H. Cozijn, E. F. G. Van Daalen, and E. A. Tannuri. Transient power control in dynamic positioning-governor feedforward and dynamic thrust allocation. In *11th IFAC Conference on Control Applications in Marine Systems, Robotics, and Vehicles*, 2018.

[52] E. Ruth, A. J. Sørensen, and T. Perez. Thrust allocation with linear constrained quadratic cost function. In *7th IFAC Conference on Control Applications in Marine Systems*, 2007.

[53] D. Zhao, F. Ding, J. Tan, Y. Liu, and X. Bian. Optimal thrust allocation based ga for dynamic positioning ship. In *2010 IEEE International Conference on Mechatronics and Automation*, 2010.

[54] T. A. Johansen, T. I. Fossen, and S. P. Berge. Constrained nonlinear control allocation with singularity avoidance using sequential quadratic programming. *IEEE Transactions on Control Systems Technology*, 12(1):211–216, 2004.

[55] C. De Wit. *Optimal thrust allocation methods for dynamic positioning of ships*. PhD thesis, Delft University of Technology, 2009.

[56] Offshore Industry Magazine. Gustomsc introduces magellan-class drillship. https://www.gustomsc.com/design/og-drilling/magellan, 2008. Accessed: 2020-01-18.

[57] F. Benetazzo, G. Ippoliti, S. Longhi, and P. Raspa. Advanced control for fault-tolerant dynamic positioning of an offshore supply vessel. *Ocean Engineering*, 106:472–484, 2015.

[58] A. Witkowska and R. Śmierzchalski. Adaptive dynamic control allocation for dynamic positioning of marine vessel based on backstepping method and sequential quadratic programming. *Ocean Engineering*, 163:570–582, 2018.

[59] T. Perez, T. I. Fossen, and A. Sorensen. A discussion about seakeeping and manoeuvring models for surface vessels. In *Centre for Ships and Ocean Structures (CESOS), Technical Report No. MSS-TR-001*, 2004.

[60] L. P. Perera, P. Oliveira, and C. G. Soares. Maritime traffic monitoring based on vessel detection, tracking, state estimation, and trajectory prediction. *IEEE Transactions on Intelligent Transportation Systems*, 13(3):1188–1200, 2012.

[61] V. Bertram. *Practical ship hydrodynamics*. Elsevier, 2011.

[62] OCIMF. Prediction of wind and current loads on vlccs. In *Oil Companies International Marine Forum London*, 1994.

[63] O. Faltinsen. *Sea loads on ships and offshore structures*. Cambridge university press, 1993.

[64] SINTEF. Shipx. https://www.sintef.no/en/software/shipx/. Accessed: 2020-02-19.

[65] M. W. C. Oosterveld. *Wake adapted ducted propellers*. PhD thesis, Delft University of Technology, 1970.

[66] F. Concli and C. Gorla. Numerical modeling of the power losses in geared transmissions: Windage, churning and cavitation simulations

with a new integrated approach that drastically reduces the computational effort. *Tribology International*, 103(1):58–68, 2016.

[67] M. Godjevac, J. Drijver, L. de Vries, and D. Stapersma. Evaluation of losses in maritime gearboxes. *Proceedings of the Institution of Mechanical Engineers, part M: Journal of Engineering for the Maritime Environment*, 230(4):623–638, 2016.

[68] R. D. Geertsma, R. R. Negenborn, K. Visser, and J. J. Hopman. Torque control for diesel mechanical and hybrid propulsion for naval vessels. In *13th international naval engineering conference*, 2016.

[69] M. Kalikatzarakis, R. D. Geertsma, E. J. Boonen, K. Visser, and R. R. Negenborn. Ship energy management for hybrid propulsion and power supply with shore charging. *Control Engineering Practice*, 76:133–154, 2018.

[70] J. Drijver. *Evaluation of transmission losses, heat flows and temperatures of propulsive drive lines*. PhD thesis, Delft university of technology, 2013.

[71] C. M. Ong. *Dynamic simulation of electric machinery using Matlab/Simulink*. Prentice-Hall PTR, 1998.

[72] P. C. Krause, O. Wasynczuk, S. D. Sudhoff, and S. Pekarek. *Analysis of electric machinery and drive systems*. Wiley Online Library, 2002.

[73] F. Blaschke. New method of regulation for rotating field machines. *Siemens Forsch Entwicklungsber*, 3(5):327–332, 1974.

[74] A. M. Trzynadlowski. *Control of induction motors*. Elsevier, 2000.

[75] G. Rizzoni, L. Guzzella, and B. M. Baumann. Unified modeling of hybrid electric vehicle drivetrains. *IEEE/ASME transactions on mechatronics*, 4(3):246–257, 1999.

[76] M. Patel. *Shipboard propulsion, power electronics, and ocean energy*. Crc Press, 2012.

[77] A.J. Wood, B.F. Wollenberg, and G.B. Sheblé. *Power generation, operation, and control*. John Wiley & Sons, 2013.

[78] H. Grimmelius, P. De Vos, M. Krijgsman, and E. van Deursen. Control of hybrid ship drive systems. In *International conference on computer and IT applications in the maritime industries*, 2011.

[79] American Bureau of Shipping. Guide for dynamic positioning systems. https://ww2.eagle.org/content/dam/eagle/rules-and-guides/archives/other/191_dpsguide/DPS_Guide_e-July14.pdf. Accessed: 2020-02-19.

[80] T. A. Johansen. Optimizing nonlinear control allocation. In *43rd IEEE Conference on Decision and Control*, 2004.

[81] O. J. Sørdalen. Optimal thrust allocation for marine vessels. *Control Engineering Practice*, 5(9):1223–1231, 1997.

[82] S. P. Berge and T. Fossen. Robust control allocation of overactuated ships; experiments with a model ship. In *4th IFAC Conference on Manoeuvring and Control of Marine Craft*, 1997.

[83] A. Mavrommati, J. Schultz, and T. D. Murphey. Real-time dynamic-mode scheduling using single-integration hybrid optimization. *IEEE Transactions on Automation Science and Engineering*, 13(3):1385–1398, 2016.

[84] Q. Duan, J. Zeng, K. Chakrabarty, and G. Dispoto. Real-time production scheduler for digital-print-service providers based on a dynamic incremental evolutionary algorithm. *IEEE Transactions on Automation Science and Engineering*, 12(2):701–715, 2014.

[85] M. G. Ardakani, B. Olofsson, A. Robertsson, and R. Johansson. Model predictive control for real-time point-to-point trajectory generation. *IEEE Transactions on Automation Science and Engineering*, 16(2):972–983, 2018.

[86] X. Chen, W. Du, H. Tianfield, R. Qi, W. He, and F. Qian. Dynamic optimization of industrial processes with nonuniform discretization-based control vector parameterization. *IEEE Transactions on Automation Science and Engineering*, 11(4):1289–1299, 2013.

[87] H. Zhang and Q. Hui. Parallel multiagent coordination optimization algorithm: implementation, evaluation, and applications. *IEEE Transactions on Automation Science and Engineering*, 14(2):984–995, 2016.

[88] E. Camponogara and H. F. Scherer. Distributed optimization for model predictive control of linear dynamic networks with control-input and output constraints. *IEEE Transactions on Automation Science and Engineering*, 8(1):233–242, 2010.

[89] Y. Song, M. T. Zhang, J. Yi, L. Zhang, and L. Zheng. Bottleneck station scheduling in semiconductor assembly and test manufacturing using ant colony optimization. *IEEE Transactions on Automation Science and Engineering*, 4(4):569–578, 2007.

[90] T. Chai, J. Ding, G. Yu, and H. Wang. Integrated optimization for the automation systems of mineral processing. *IEEE Transactions on Automation Science and Engineering*, 11(4):965–982, 2014.

[91] D. Zhang, P. B. Luh, J. Fan, and S. Gupta. Chiller plant operation optimization: Energy-efficient primary-only and primary-secondary systems. *IEEE Transactions on Automation Science and Engineering*, 15(1):341–355, 2017.

[92] N. Kamra, S. Kumar, and N. Ayanian. Combinatorial problems in multirobot battery exchange systems. *IEEE Transactions on Automation Science and Engineering*, 15(2):852–862, 2017.

[93] M. A. Bragin, P.B. Luh, B. Yan, and X. Sun. A scalable solution methodology for mixed-integer linear programming problems arising in automation. *IEEE Transactions on Automation Science and Engineering*, 16(2):531–541, 2018.

[94] B. Yan, P. B. Luh, G. Warner, and P. Zhang. Operation and design optimization of microgrids with renewables. *IEEE Transactions on Automation Science and Engineering*, 14(2):573–585, 2017.

[95] D. Ashlock. *Evolutionary computation for modelLing and optimization*. Springer Science & Business Media, 2006.

[96] O. Kramer. *Genetic algorithm essentials*, volume 679. Springer, 2017.

[97] R. A. Waltz, J. L. Morales, J. Nocedal, and D. Orban. An interior algorithm for nonlinear optimization that combines line search and trust region steps. *Mathematical programming*, 107(3):391–408, 2006.

[98] H. Lau, T. M. Chan, W. T. Tsui, and W. K. Pang. Application of genetic algorithms to solve the multidepot vehicle routing problem. *IEEE transactions on automation science and engineering*, 7(2):383–392, 2009.

[99] C. W. Chou, C. F. Chien, and M. Gen. A multiobjective hybrid genetic algorithm for tft-lcd module assembly scheduling. *IEEE Transactions on Automation Science and Engineering*, 11(3):692–705, 2014.

[100] P. K. Jamwal, S. Hussain, and S. Q. Xie. Three-stage design analysis and multicriteria optimization of a parallel ankle rehabilitation robot using genetic algorithm. *IEEE Transactions on Automation Science and Engineering*, 12(4):1433–1446, 2014.

[101] F. Qiao, Y. Ma, L. Li, and H. Yu. A petri net and extended genetic algorithm combined scheduling method for wafer fabrication. *IEEE Transactions on Automation Science and Engineering*, 10(1):197–204, 2012.

[102] J. Song, Y. Qiu, and Z. Liu. Integrating optimal simulation budget allocation and genetic algorithm to find the approximate pareto patient flow distribution. *IEEE Transactions on Automation Science and Engineering*, 13(1):149–159, 2015.

[103] K. De Jong. Learning with genetic algorithms: An overview. *Machine learning*, 3(3):121–138, 1988.

[104] K. Deep, K. P. Singh, M. L. Kansal, and C. Mohan. A real coded genetic algorithm for solving integer and mixed integer optimization problems. *Applied Mathematics and Computation*, 212(2):505–518, 2009.

[105] K. Deb. An efficient constraint handling method for genetic algorithms. *Computer methods in applied mechanics and engineering*, 186(2-4):311–338, 2000.

[106] A. Conn, N. Gould, and P. Toint. A globally convergent lagrangian barrier algorithm for optimization with general inequality constraints and simple bounds. *Mathematics of Computation*, 66(217):261–288, 1997.

[107] R. Eberhart and J. Kennedy. Particle swarm optimization. In *IEEE international conference on neural networks*, 1995.

[108] Y. Shi and R. Eberhart. A modified particle swarm optimizer. In *IEEE international conference on evolutionary computation*, 1998.

[109] S. Koziel and S. Yang. *Computational optimization, methods and algorithms*. Springer, 2011.

[110] X. Hu and R. Eberhart. Solving constrained nonlinear optimization problems with particle swarm optimization. In *6th world multiconference on systemics, cybernetics and informatics*, 2002.

[111] C. M. Martinez and D. Cao. *iHorizon-Enabled Energy management for electrified vehicles*. Butterworth-Heinemann, 2018.

[112] R. Eberhart and Y. Shi. Comparing inertia weights and constriction factors in particle swarm optimization. In *Congress on evolutionary computation*, 2000.

[113] A. El-Gallad, M. El-Hawary, A. Sallam, and A. Kalas. Enhancing the particle swarm optimizer via proper parameters selection. In *Canadian Conference on Electrical and Computer Engineering*, 2002.

[114] M. Iwamatsu. Locating all the global minima using multi-species particle swarm optimizer: The inertia weight and the constriction factor variants. In *IEEE International Conference on Evolutionary Computation*, 2006.

[115] W. Han, P. Yang, H. Ren, and J. Sun. Comparison study of several kinds of inertia weights for pso. In *IEEE International Conference on Progress in Informatics and Computing*, 2010.

[116] A. Ratnaweera, S. K. Halgamuge, and H. C. Watson. Self-organizing hierarchical particle swarm optimizer with time-varying acceleration coefficients. *IEEE Transactions on evolutionary computation*, 8(3):240–255, 2004.

[117] T. Yamaguchi and K. Yasuda. Adaptive particle swarm optimization; self-coordinating mechanism with updating information. In *IEEE International Conference on Systems, Man and Cybernetics*, 2006.

[118] J. J. Liang, A. K. Qin, P. N. Suganthan, and S. Baskar. Comprehensive learning particle swarm optimizer for global optimization of multimodal functions. *IEEE transactions on evolutionary computation*, 10(3):281–295, 2006.
[119] M. Clerc and J. Kennedy. The particle swarm-explosion, stability, and convergence in a multidimensional complex space. *IEEE transactions on Evolutionary Computation*, 6(1):58–73, 2002.
[120] K. R. Frisch. The logarithmic potential method of convex programming. In *Memorandum of University Institute of Economics, Oslo*, 1955.
[121] N. Karmarkar. A new polynomial-time algorithm for linear programming. In *16th annual ACM symposium on Theory of computing*, 1984.
[122] S. L. Bales. Wave and wind data for seakeeping performance assessment. In *The International Towing Tank Conference, Seakeeping Committee*, 1983.
[123] J. Heywood. Internal combustion engine fundamentals. 1988.

Miltiadis Kalikatzarakis received his M.Eng. in Naval Architecture and Marine Engineering from the National Technical University of Athens (2013), and his MSc. in Marine Technology from the Delft University of Technology (2017). He joined the Research & Development department of Damen Schelde Naval Shipbuilding in 2017, and has been involved in data analytics, modeling and design optimisation in the maritime industry.

Andrea Coraddu is a Assistant Professor in Marine Engineering in the Department of Naval Architecture, Ocean and Marine Engineering (NAOME) at the University of Strathclyde, Glasgow. His primary research involves on-board data in assessing vessel performance, energy optimisation, and real-time monitoring of the primary systems. Utilising the latest learning algorithms and theoretical results in machine learning, Dr Coraddu is developing data-driven approaches to investigate the behaviour of complex on-board systems and their interaction.

Luca Oneto was born in Rapallo, Italy in 1986. He received his BSc and MSc in Electronic Engineering at the University of Genoa, Italy respectively in 2008 and 2010. In 2014 he received his PhD from the same university in the School of Sciences and Technologies for Knowledge and Information Retrieval with the thesis "Learning Based On Empirical Data". In 2018 he was co-funder of the spin-off ZenaByte s.r.l. In 2019 he became Associate Professor in Computer Science at University of Pisa and currently is Associate Professor in Computer Engineering at University of Genoa. He has been involved in several H2020 projects (S2RJU, ICT, DS) and he has been awarded with the Amazon AWS Machine Learning and Somalvico (best Italian young AI researcher) Awards. His first main topic of research is the Statistical Learning Theory with particular focus on the theoretical aspects of the problems of (Semi) Supervised Model Selection and Error Estimation. His second main topic of research is Data Science with particular reference to the problem of Trustworthy AI and the solution of real world problems by exploiting and improving the most recent Learning Algorithms and Theoretical Results in the fields of Machine Learning and Data Mining.

Davide Anguita received the 'Laurea' degree in Electronic Engineering and a Ph.D. degree in Computer Science and Electronic Engineering from the University of Genoa, Genoa, Italy, in 1989 and 1993, respectively. After working as a Research Associate at the International Computer Science Institute, Berkeley, CA, on special-purpose processors for neurocomputing, he returned to the University of Genoa. He is currently Associate Professor of Computer Engineering with the Department of Informatics, BioEngineering, Robotics, and Systems Engineering (DIBRIS). His current research focuses on the theory and application Artificial Intelligence.